Tosi Federico (Orcid ID: 0000-0003-4002-2434)
Mura Alessandro (Orcid ID: 0000-0002-4552-4292)
Lopes Rosaly (Orcid ID: 0000-0002-7928-3167)
Filacchione Gianrico (Orcid ID: 0000-0001-9567-0055)
Ciarniello Mauro (Orcid ID: 0000-0002-7498-5207)
Zambon Francesca (Orcid ID: 0000-0002-4190-6592)
Adriani Alberto (Orcid ID: 0000-0003-4998-8008)
Brooks Shawn, M. (Orcid ID: 0000-0001-8622-0829)
Noschese Raffaella (Orcid ID: 0000-0003-0502-0337)
Turrini Diego (Orcid ID: 0000-0002-1923-7740)
Altieri Francesca (Orcid ID: 0000-0002-6338-8300)
Cicchetti Andrea (Orcid ID: 0000-0002-9588-6531)
Grassi Davide (Orcid ID: 0000-0003-1653-3066)
Hansen Candice, J. (Orcid ID: 0000-0001-5863-299X)
Migliorini Alessandra (Orcid ID: 0000-0001-7386-9215)
Moriconi Maria, L. (Orcid ID: 0000-0003-2609-2620)
Piccioni Giuseppe (Orcid ID: 0000-0002-7893-6808)
Plainaki Christina (Orcid ID: 0000-0003-1483-5052)

Mapping Io's Surface Composition with Juno/JIRAM

F. Tosi[1], A. Mura[1], R. M. C. Lopes[2], G. Filacchione[1], M. Ciarniello[1], F. Zambon[1], A. Adriani[1], S. J. Bolton[3], S. M. Brooks[2], R. Noschese[1], R. Sordini[1], D. Turrini[1], F. Altieri[1], A. Cicchetti[1], D. Grassi[1], C. J. Hansen[4], A. Migliorini[1], M. L. Moriconi[5], G. Piccioni[1], C. Plainaki[6], G. Sindoni[6]

[1] Istituto Nazionale di AstroFisica – Istituto di Astrofisica e Planetologia Spaziali (INAF-IAPS), Rome, Italy.

[2] Jet Propulsion Laboratory, California Institute of Technology, Pasadena, California, USA.

[3] Space Science and Engineering Division, Southwest Research Institute, San Antonio, Texas, USA.

[4] Planetary Science Institute, Tucson, Arizona, USA.

[5] CNR-Istituto di Scienze dell'Atmosfera e del Clima, Rome, Italy.

[6] Agenzia Spaziale Italiana, Rome, Italy.

Corresponding author: Federico Tosi (federico.tosi@inaf.it)

Key Points:

- We use spectra acquired by Juno/JIRAM in the range 2–5 μm over a three-year period, covering ~22% of Io, to map its surface composition.

This article has been accepted for publication and undergone full peer review but has not been through the copyediting, typesetting, pagination and proofreading process which may lead to differences between this version and the Version of Record. Please cite this article as doi: 10.1029/2020JE006522

- The 2.1-µm band and the 2.65-µm band are unrelated with SO_2 frost, but display trends possibly related to the transport of volatiles.
- We confirm that the 4.47-µm band is diagnostic of $^{32}S^{16}O^{18}O$, and we show that $ClSO_2$ is not everywhere linked to the abundance of Cl_2SO_2.

Abstract

The surface composition of Io is dominated by SO_2 frost, plus other chemical species identified or proposed over the past decades by combining Earth-based and space-based observations with laboratory data. Here we discuss spectroscopic datasets of Io obtained by the JIRAM spectro-imager onboard Juno in nine orbits, spanning a three-year period. We display average spectral profiles of Io in the 2–5 μm range and we use band depths derived from those profiles to map the geographic distribution of SO_2 frost and other spectral features. This dataset allows for a ~22% surface coverage at 58 to 162 km/px, and in a broad range of latitudes. Our results confirm the broadly regional SO_2-frost trends already highlighted by Galileo/NIMS. Io's average spectral profiles as well as the mapping of the 4.47-μm band also confirm that SO_2 exists in the $^{32}S^{16}O^{18}O$ isotopic form. Surprisingly, the mapping performed by JIRAM shows that the absorption band at 2.1 μm is unrelated to SO_2 frost, while we map for the first time the depth of the 2.65-μm band, highlighting regions enriched in this absorber, possibly H_2S. JIRAM data confirm that the 3.92-μm band, likely due to Cl_2SO_2, is largely related to the SO_2 distribution. The correlation between Cl_2SO_2 and $ClSO_2$, possibly revealed at 4.62 μm, is not equally clear. The simultaneous presence of two very weak spectral features at 4.55 and 4.62 μm suggests that nitrile compounds or tholins may also be present on the surface.

Plain Language Summary

The surface of Io is mainly covered by sulfur dioxide (SO_2) frost, and by other chemical species. The JIRAM instrument onboard the NASA Juno spacecraft, in orbit around Jupiter, can occasionally observe the Galilean satellites through its slit spectrometer (2–5 μm range). We show average spectral profiles of Io obtained by JIRAM in a three-year period, mapping the geographic distribution of SO_2 frost and other spectral features. Our results confirm the broadly regional SO_2-frost trends already highlighted in the past. Our data confirm that SO_2 exists in multiple isotopic forms. Surprisingly, the mapping performed by JIRAM shows that the absorption band at 2.1 μm is unrelated to SO_2 frost. We map for the first time the depth of the 2.65-μm band, which might be related to hydrogen sulfide (H_2S). We also highlight regions enriched in this absorber. We confirm that the 3.92-μm band, ascribed to sulfuryl chloride (Cl_2SO_2), is largely correlated with the SO_2 distribution. The correlation between Cl_2SO_2 and $ClSO_2$, possibly revealed at 4.62 μm, is not equally clear. The simultaneous presence of two very weak spectral features at 4.55 and 4.62 μm suggests that nitrile compounds or tholins may also be present on the surface.

1 Introduction and Background

Telescopic spectra acquired since the 1970s, compared with laboratory measurements, clearly demonstrated the widespread occurrence of sulfur dioxide frost on the surface of Io, plus some spectrally neutral material, possibly sulfur, confirmed by the multispectral images returned by Voyager probes (e.g. Smythe et al., 1979; Fanale et al., 1979; Cruikshank, 1980; Howell et al., 1984; Cruikshank et al., 1985). In the near infrared range, SO_2 frost exhibits two very strong signatures at 4.07 μm and 4.37 μm, respectively ascribed to the combination $\nu_1 + \nu_3$ and the overtone $2\nu_1$ of the SO_2 molecule, in addition to other six weaker features centered at approximately 2.54 μm (overtone $3\nu_3$), 2.79 μm (combination $2\nu_1 + \nu_3$), 2.92 μm (overtone $3\nu_1$), 3.35 μm (combination $\nu_1 + \nu_2 + \nu_3$), 3.56 μm (combination $2\nu_1 + \nu_2$), and 3.78 (overtone $2\nu_3$) (Nash and Betts, 1995, 1998).

Reflectance spectroscopy of Io's SO_2 surface frosts in the 3–5 μm range had been used to infer the strengths of ^{33}S, ^{34}S, and ^{18}O (Howell et al., 1989), and laboratory spectra shown in

the same work ruled out the possible presence of $NaSO_4$ and $NaSO_3$. On the other hand, it was possible to identify new spectral signatures in the infrared telescopic spectra of Io, e.g. a pair of weak bands centered at around 3.85 and 3.92 μm (Howell et al., 1989) and another pair of signatures centered at 2.97 and 3.15 μm, respectively (Salama et al., 1990). In principle, the 3.92- and 3.85-μm bands could be accounted for by the absorption of the S-H stretching vibration (ν_1) in hydrogen sulfide (H_2S) present as clusters and isolated molecules in an SO_2-dominated ice (Salama et al., 1990). The weak 2.97- and 3.15-μm bands, found to vary spatially and temporally in the Io spectra coincide with the ν_3 and ν_1 O-H stretching vibrations of clusters of water (H_2O) complexed, through hydrogen bonding and charge transfer interactions, with SO (Salama et al., 1990).

On the basis of telescopic observations, Trafton et al. (1991) first identified a new absorption band centered at approximately 2.1 μm, which was tentatively identified with the spectral counterpart of the $2\nu_3$ overtone of CO_2 multimers or "clusters" buried within an SO_2 frost-dominated surface (Sandford et al., 1991, 1993). In this regard, Schmitt et al. (1994) later proposed the 2.1 μm feature to be the SO_2 $3\nu_1 + \nu_3$ mode. If the CO_2 hypothesis were verified, then the spectral counterpart of the ν_3 $^{12}CO_2$ asymmetric stretch fundamental at 4.26 μm should be observed in addition to two weaker spectral signatures centered respectively at 2.70 μm (combination $\nu_1 + \nu_3$) and 2.78 μm (combination $2\nu_2 + \nu_3$). However, in Io spectra, the 2.78-μm region is masked by the $2\nu_1 + \nu_3$ combination of SO_2, and at 2.70 μm there is only a hint of a potential inflection.

These early findings immediately posed the question of whether volatile compounds such as hydrogen sulphide, water and carbon dioxide were endogenous or exogenous in origin, and how could they condense and survive on the surface of Io. For example, while H_2S, H_2O and CO_2 are commonly emitted in volcanic eruptions on Earth along with SO_2, a plausible exogenic source could conceivably form H_2S and H_2O by insertion of highly energetic H^+ ions in the SO_2 ice surface under the heavy bombardment of the satellite by the atoms (Salama et al., 1990). Furthermore, residence times are influenced by the typical environmental conditions both in terms of temperature and of radiation environment.

Continued space exploration carried out by the NASA Galileo spacecraft from 1996 to 2002, thanks to the NIMS imaging spectrometer (Carlson et al., 1992) allowed mapping the surface composition of Io in the near infrared range 0.7-5.2 μm, with an average spectral sampling of 25 nm longward of 1 μm and an unprecedented level of detail. In addition to confirming some of the results previously obtained from Earth-based observations, NIMS was able to discover that, despite SO_2 frost being widespread on Io's surface, it is actually very unevenly distributed, with the highest areal abundances at medium and high latitudes. The central region of hot volcanic vents showed substantial depletion, because high surface temperatures promote rapid vaporization and can produce SO_2-free areas (Carlson et al., 1997). NIMS confirmed the presence of a weak but persistent absorption feature at 3.15 μm, tentatively attributed to hydroxides, hydrates, or water.

Based on 10 hyperspectral NIMS images, Douté et al. (2001) accurately mapped the SO_2 frost distribution over 60% of the satellite surface, confirming that this compound is indeed omnipresent at the coarse spatial scale typical of NIMS data in the early part of the mission (~200 km), but with remarkable inhomogeneities. Consistent with the early result obtained by Carlson et al. (1997), they found that SO_2 frost tends to accumulate at medium to high latitude, although the majority of known plumes erupt near the equator. Furthermore, SO_2 frost is more abundant on Io's leading side than on the trailing side. It is possible that the differences in opacity and porosity in the uppermost surface layer between the two hemispheres, the trailing hemisphere being darker than the leading hemisphere, are a consequence of this distribution.

While plumes detected by Voyager and Galileo are the principal sources of gaseous SO_2, the dynamic condensation, remobilization, transport, and final condensation phases that follow the emission of SO_2 by the plumes form different and very distinctive physical units of frost at the surface.

In a second work, Douté et al. (2002) analyzed a series of NIMS spectral image cubes acquired with much better spatial resolution, ranging from 7 to 25 km/px, but with significantly poorer spectral resolution, and covering Prometheus patera, a 28-km volcanic depression originating a 100-km long lava flow field, located at the equator on the anti-Jovian hemisphere. They used SO_2 frost as a tracer to understand various thermodynamic and volcanic processes acting in this equatorial region and, as a result, obtained reliable and consistent maps of local SO_2 abundance and granularity, highlighting the existence of four different physical units (I: high frost coverage and fine grains; II: high frost coverage and coarse grains; III: depleted in SO_2 and fine-grained, and IV: moderate SO_2 areal abundance and large grain sizes), whose distribution indicates zones of condensation, metamorphism, and sublimation linked with the thermodynamic and volcanic processes of interest. They speculated that after a possible dynamic condensation around the plumes or at the equator, the gas is remobilized by the solar or thermal fluxes and flows mostly latitudinally toward the coldest and nearest regions devoid of hot-spots.

In a third work, Douté et al. (2004) followed up the mapping of SO_2 abundance and granularity in new NIMS data acquired at spatial resolution between 3 and 46 km/px (though using only 12 wavelengths due to a radiation-induced anomaly), correlating those data to emphasize the four homogeneous units previously found by Douté et al. (2002). Northwest of Gish Bar Patera, a localized bright deposit interestingly showed an unusual spectral signature at 3.0 µm, in the continuum wing of the 3.15-µm feature, suggestive of very fine-grained H_2O molecules forming ice crystals or being intimately mixed within a nonidentified, bright neutral matrix, since no other signatures diagnostic of water ice show up at 2.0 and 1.5 µm. Granahan (2004) also detected a very weak 3.0-µm feature on the plateaus of Tvashtar Montes, in the Tvashtar caldera, in the massif of Tohil Mons, and around Gish Bar Patera. All of these localities and morphologic features are associated with some of Io's mountains. Indeed, iron sulfide minerals like pyrite and marcasite (FeS_2) and/or pyrrhotite ($Fe_{1-x}S$) could be responsible for the 3.0-µm absorption if this is observed along with another, much broader absorption close to 1 µm (Carlson et al., 2007).

Sodium was expected to be present in some form on the surface, having been discovered in the Io torus (Brown, 1974). Sodium chloride (NaCl) was finally observed in volcanic plumes (Lellouch et al., 2003). Based on data collected by the Cosmic Dust Analyser onboard the Cassini Orbiter (Srama et al., 2004) during the Jupiter Millennium flyby which occurred in late 2000, NaCl was confirmed to be the major particle constituent of the observed stream particles originating from Io, accompanied by sulphur- as well as potassium-bearing components (Postberg et al., 2006). Starting from the discovery of chlorine ions in Io's plasma torus, Schmitt and Rodriguez (2003) searched for evidence of Cl-bearing species at the surface of the satellite. They identified sulfuryl chloride (Cl_2SO_2) diluted at ~1% in a millimeter-thick layer of solid SO_2 as the best candidate for the 3.92-µm band locally present in NIMS spectra. H_2S diluted in SO_2 in principle could also fit the 3.92-µm band, but is extremely unstable at Io's surface. H_2S displays an additional strong component at 3.85 µm, which had been first reported by Howell et al. (1989) but was not observed later in NIMS data. Besides Cl_2SO_2, a potential contribution coming from $ClSO_2$ is suggested by a diagnostic absorption band centered at 4.62 µm (Schmitt & Rodriguez, 2003), which had been widely observed on Io by Soderblom et al. (1999) and alternatively proposed to be due to some form of sulfate or cyanides (Carlson et al., 2007).

Currently, isotopic studies on Solar System satellites are limited to gas species that can be detected in situ with a mass spectrometer or remotely via spectroscopy, and in certain cases to surface frosts via reflectance spectroscopy. On Io, sulfur isotope studies offer an additional avenue, and preliminary measurements of sulfur isotopes in SO_2 have already been made (Moullet et al., 2013). For instance, Soderblom et al. (1999) and Baklouti (2006) suggested that a 4.48-μm absorption feature on Io could be the $2\nu_1$ overtone of SO_2 in the form of $^{32}S^{16}O^{18}O$. Alternatively, the 4.48-μm band might be ascribed to an overtone/combination of the hydroxonium molecule H_3O^+ in sulfuric acid tetrahydrate, $H_2SO_4{\cdot}4H_2O$, which is a product of radiolysis of SO_2 and H_2S in water ice (Moore et al., 2007). Furthermore, comparison of sulfur isotope ratios between objects in the Jupiter system, including Europa and Jupiter itself, may provide information about the exogenic vs. endogenic nature of the S seen on these other bodies.

On Io as well as the icy satellites, the surface is the source for the (non-directly-outgassed) atmospheric material, and a comparison of atmospheric ratios between the surface frosts and atmospheric gasses would provide key information on fractionation due to the processes that remove material from the surface (sublimation, sputtering, etc.), and on potential vertical isotopic fractionation gradients in the atmosphere. Spatial mapping of isotope ratios across the surfaces of these objects may also probe the temporal axis, as the expected surface frost deposition age varies latitudinally (de Kleer et al., 2019).

Spatially resolved spectroscopic observations of Io by the Hubble Space Telescope provided direct evidence that, similar to the abundance of SO_2 frost on the surface, the Io atmosphere is also spatially inhomogeneous (McGrath et al., 2000). SO_2 gas dominates the tenuous atmosphere of Io, and the sunlit SO_2 atmosphere is globally stable with minor local variability (Feaga et al., 2009). Besides SO_2 gas, SO is likely to be present, along with S_2 (Spencer et al., 2000). Also likely to be present are S_3 and S_4 formed by heating of sulfur and by ultraviolet photolysis of S_2, followed by S_8 by polymerization within the plumes or on the surface (Carlson et al., 2007). Diffuse red deposits in Pele's red plumes deposits and near other Io volcanoes suggest that venting and polymerization of S_2 gas is a widespread feature of Io volcanism (Spencer et al., 2000).

In previous work based on Juno/JIRAM data, a series of preliminary results obtained at Io by the JIRAM spectro-imager were presented (Mura et al., 2020). These results range from monitoring the volcanic activity of Io and discovering new hot spots located in the southern polar region by means of infrared images to measuring the average surface composition and mapping the surface temperature of hot spots by using spectroscopic data sets.

Here we focus on the surface composition of Io as derived by JIRAM spectroscopic data in the near-infrared range 2–5 μm. This spectral range is not large enough to allow the detection of all the spectral signatures discovered on Io over the last decades, but it does allow determining the geographic distribution of the main chemical species revealed in this spectral range at the time of Juno observations. In particular, in addition to the signatures that are firmly assigned to SO_2 frost and are centered at 2.54, 2.79, 2.92, 3.35, 3.55, 3.78, 4.07 and 4.37 μm, from the previous work by Mura et al. (2020) it emerged how other spectral signatures show up in JIRAM-derived spectral profiles. They report spectral features centered at 3.92 μm and 4.62 μm, respectively attributed to Cl_2SO_2 and possibly to $ClSO_2$, as well as a signature at 4.47 μm that may be attributable to either to specific isotopes of sulfur and oxygen, such as $^{32}S^{16}O^{18}O$, or alternatively to the presence of H_3O^+ in a matrix of $H_2SO_4{\cdot}4H_2O$. In addition to these, there are other recurring signatures in JIRAM spectra, e.g. the 2.1-μm spectral feature which was initially attributed to CO_2 and then to SO_2. In this case, while the SO_2 hypothesis is easier to support, the distribution of the 2.1-μm spectral signature shall be compared with the

distribution of other stronger SO_2 absorption features to make sure this is really the most plausible explanation.

JIRAM spectroscopic data sets also show evidence for a very weak, recurrent absorption band centered at 2.65-μm, which has been first pointed out by Mura et al. (2020). Since this wavelength does not correspond to any known JIRAM artifact, if we assume that it is real, it is reasonable to ask what it is due to and whether this signature displays any relationship with the geographic location of known geologic features as well as with other chemical species known or proposed to exist on the surface of Io. The same applies to a spectral signature centered at 4.55 μm, which is recurrently observed in JIRAM spectra of Io. However, at a slightly different wavelength (4.57 μm), a feature had previously been reported also on Callisto and Ganymede based on NIMS data, and proposed to be the spectral counterpart of the CN bond in nitrile compounds or tholins (McCord et al., 1997, 1998).

In this work we investigate those spectral signatures that are recurrent in the average JIRAM spectral data sets acquired from March 2017 until April 2020, with the goal of mapping their geographic distribution at the typical spatial scale achieved in this three-years period. Since Juno moves around Jupiter on a polar orbit, these spectroscopic observations are valuable in that they follow up and complement four decades of previous observations, especially at high latitudes that are inaccessible from Earth-based observations, and that Galileo NIMS observed poorly. The Juno mission profile ensures that Io can be observed quite frequently close to perijoves, which allow both the monitoring of its volcanic activity and the possibility of mapping its surface composition and comparing it with previous findings. The mapping of different chemical species is also key to defining any potential relationships existing between them, thus allowing one to shed light on their nature, particularly their link to an SO_2 frost matrix in the uppermost surface layer as thick as 1 mm.

In Section 2 of this article we briefly describe the JIRAM instrument. In Section 3 we discuss the JIRAM data sets used for our analysis and the method followed to analyse them. We display the average Io spectral profiles acquired in different orbits, highlighting the spectral signatures that show up and discussing the variability of the data sets. In Section 4 we report on the results we obtained in terms of geographic distribution of the band depth values measured for a number of spectral signatures, investigating correlations arising between such maps and emphasizing the original contribution provided by JIRAM with respect to previous works.

2 The JIRAM instrument

The Jovian InfraRed Auroral Mapper (JIRAM) is a spectro-imager onboard the Juno spacecraft, which entered orbit around Jupiter in July 2016 (Bolton et al., 2017). This instrument was designed specifically to explore the Jovian auroral regions and the planet's atmospheric structure, dynamics and composition (Adriani et al., 2017).

JIRAM is essentially composed of two subsystems, or channels: an imager and a slit spectrometer, sharing the same telescope, a de-spinning mirror to compensate the smearing induced by the spin of the spacecraft, and an internal calibration unit. The imaging subsystem (IMG) is split into two equal areas defined by two adjacent band-pass filters: an L filter, centered at 3.45 μm with a 290 nm bandwidth, and an M filter, centered at 4.78 μm with a 480 nm bandwidth (Adriani et al., 2017). Each channel has a Field of View (FOV) of 5.87° by 1.74° (432 × 128 pixels corresponding to the across and along track directions, respectively) and an Instantaneous Field of View (IFOV), or angular resolution, of about 240 × 240 μrad.

The spectrometer channel (SPE) is co-located on line 13 of the M-band imager's FOV and can acquire spectra in the 2.0-5.0 μm range by using a slit of 256 spatially contiguous

pixels (samples) with a FOV of 3.5° and an IFOV of about 240 μrad. The slit's image is dispersed by a grating across the focal plane and sampled along the detector's 336 columns in the spectral range 2–5 μm, resulting in an average spectral sampling of 9 nm/band. Thus the typical high spatial/high spectral instantaneous acquisition of the SPE channel is a frame made up of a 256 spatial pixels × 336 spectral pixels (spectels). While the on-ground calibration of JIRAM is extensively described in Adriani et al. (2017), periodic in-flight calibration is performed by observing internal calibration sources as well as the sky background to characterize and monitor long-term variations in terms of spectral responsivity, thermal background, and readout noise, which are affected by the local environment. In particular, following the Earth-Moon flyby which occurred in October 2013 (Adriani et al., 2016), and in the cruise phase to Jupiter by using Aldebaran and the Galilean moons, JIRAM data allowed improvement of its absolute geometric and radiometric calibration. The Noise Equivalent Spectral Radiance (NESR) in the SPE channel has a typical value ranging between 10^{-4} and 10^{-3} W/(m^2 sr μm), with higher (i.e., worse) values concentrating in the wings of the sensitivity range. Substantial radiometric calibration residuals still remain between 2.00 and 2.02 μm, and longward of 4.8 μm.

Because Juno is a spinning spacecraft nominally rotating at ~2 rpm, or ~12 degrees per second, a flat de-spinning mirror, placed at the JIRAM telescope's entrance pupil, compensates for the spacecraft rotation and allows the target image to be kept in the field of view during the data acquisition. The instrument uses attitude information from the spacecraft to compute the required compensating rotation rate for the mirror, as well as the pointing direction. This enables exposure times up to 1 second on images and spectra without incurring in substantial smearing effects (Adriani et al., 2017).

JIRAM is very flexible in its operations: images can be acquired either in the L or M filter, or in both filters at the same time. Similarly, spectral data can be complemented by simultaneous context infrared images, or taken alone. In this regard, based on the planning and the scientific priority assigned during each passage through perijove, JIRAM can apply the most appropriate observational strategy to achieve the planned scientific objective (Noschese et al., 2020).

JIRAM can acquire only one spectral slit per Juno spacecraft rotation (i.e. 1 slit every ~30 s). Due to the combination of high spacecraft orbital velocity, low repetition rate and limited on-board software processing time, the ground footprints of the JIRAM spectrometer's consecutive slit acquisitions are generally disconnected or overlapped across the target's surface, depending upon the timing of the measurements. However, repeated observations combined with an optimized pointing strategy can ultimately fill gaps and allow substantial uniformity in coverage.

In the framework of the Juno mission, the Galilean satellites are targets of opportunity: all orbits are designed for Jupiter science, and to preserve a power-optimized attitude, targeted observations of planetary objects other than Jupiter cannot be usually planned, so JIRAM can observe the satellites only if they incidentally fall within its FOV. However, JIRAM usually operates during relatively short periods surrounding each Juno perijove passage, which occurs every ~53 days during the prime mission. Therefore it can take advantage of the frequent observation opportunities of some Galilean moons as the spacecraft flies through the inner portion of the Jovian system to collect infrared images and spectra of their surfaces. Other remote sensing instruments onboard Juno, such as JunoCam and UVS, have larger IFOVs (i.e., coarser angular resolution) compared to JIRAM's 240 μm IFOV, making JIRAM particularly suited to observe the satellites. Indeed, such opportunities have been so far exploited to observe

Europa (Filacchione et al., 2019), Io (Mura et al., 2020), and Ganymede (Mura, this special issue).

In Juno's polar orbit around Jupiter, the spacecraft approaches the planet from the north and, after passing through the perijove point, moves away from it towards the south. For this reason, the Galilean satellites can be observed both in their northern (in the inbound flyby phase) and southern hemispheres (in the outbound phase). The geometric configuration is such that the solar phase angle (Sun-satellite-Juno angle) is close to 90° on average, so that only half of the satellite is illuminated while the other half is in shadow (total eclipses by Jupiter may also occur).

3 JIRAM data sets and Methods

In this section we discuss the spectroscopic data of Io acquired by JIRAM's spectrometer channel (JIRAM-SPE, hereafter JIRAM). In the three-year period between February 2017 and April 2020, i.e. between the perijove of orbit 4 (sequence JM0041) and the perijove of orbit 26 (sequence JM0261), JIRAM was able to observe Io about 1100 times, of which 450 used also its spectrometer. As a result, Io is currently the second Galilean satellite most observed by Juno, after Ganymede and before Europa.

Here we neglect JIRAM data of Io acquired during the perijoves of orbits 4 and 6 due to the large distance of the spacecraft, which resulted in a fairly coarse spatial resolution (186 km/px and 287 km/px on average, respectively), unsuited to perform a spatial mapping of absorption band depths other than those diagnostic of SO_2 frost, which is ubiquitous at this spatial scale. We also discarded JIRAM data acquired on orbit 11, because they are few and very noisy. Orbit 16 only includes infrared images, not spectra. Finally, on orbit 25, JIRAM observed Io when it was in eclipse, with active volcanic spots standing out with respect to a completely shadowed surface. Ultimately, we retained the spectroscopic data acquired in nine orbits: 5, 7, 9, 10, 17, 18, 20, 24 and 26, which show a fair compromise in terms of spatial resolution, solar illumination and signal-to-noise ratio (SNR). In this regard, in each data set we have limited the solar incidence angle and the emission angle to values lower than 75°, in order to rule out extreme conditions in terms of grazing solar illumination and warping of the JIRAM ground footprints due to the proximity to the satellite's limb, which can both degrade the signal quality.

Starting from these initial assumptions, Table 1 reports geometric circumstances related to JIRAM observations of Io, considering only spectroscopic data sets that are the subject of this work and neglecting infrared imagery. SPICE-based routines (Acton, 1996) and navigational databases, the so-called "SPICE kernels", provide illumination conditions at any time along the orbit. Uncertainties remain in the reconstructed geometry information for the orbit 24 Io observations, which were preceded by a dedicated Ganymede observation campaign that required a reorientation of the spacecraft (see Mura et al., this issue). These uncertainties arise from a wobbling, or nutation, that was induced by the turn back to Juno's nominal orientation and is not accounted for in the reconstructed attitude information. However, our choice to retain only those data acquired with an emission angle <75° is conservative enough to ensure that all JIRAM footprints fall entirely on the Io surface. In all other cases, the accuracy on the reconstruction of the geometry is the same as the spatial resolution at the surface, i.e. one pixel.

From this table it turns out that Io spectra have been observed at pixel resolutions ranging between 58 and 162 km and solar phase angle values overall ranging between 54° and 122°. The duration of an observing sequence spanned from a minimum of 6 minutes to a maximum of 52 minutes depending on the orbit, which resulted in a variable spatial coverage,

revealed by the angular excursion of the planetocentric coordinates of the sub-spacecraft point combined with the spatial resolution. In this regard, a satisfactory coverage was achieved on the pro-Jovian (sub-Jovian) side around the prime meridian across a broad range of latitudes, while large gaps are found in the anti-Jovian trailing hemisphere. This is the result of typical geometric conditions met by the spacecraft close to perijove, with Juno's orbital period (~53 days) which is roughly 30 times Io's orbital period (1.77 days, synchronized with its rotation period). The largest illuminated fraction and the most favourable solar incidence and emission angles were met in orbit 9, which covered the southern hemisphere at an average resolution of ~103 km/px. On the other hand, the best pixel resolution (~58 km) so far has been achieved on orbit 26 (April 2020). Lastly, most observations covered the morning fraction of the dayside compared to the afternoon side.

Figure 1a shows the average spectra of Io for each orbit, expressed in units of calibrated radiance factor I/F, i.e. spectral radiance divided by a solar radiance spectrum scaled by the heliocentric distance of Io at the time of the observation. In our case, we used the high-resolution MODTRAN extraterrestrial solar irradiance based on combinations of measured and modeled data from multiple sources (https://www.nrel.gov/grid/solar-resource/spectra.html#paneld10e138_1), convoluted for the response of the individual spectral channels of the JIRAM spectrometer (Adriani et al., 2017). The average I/F spectra are obtained after filtering all data for solar incidence and emission angle values <75°, and are not corrected for any photometric function. A boxcar average over contiguous pairs of spectral channels is applied in I/F spectral profiles, to limit the so-called "odd-even" effect. This arises from an inhomogeneous readout noise of the even and odd columns of the JIRAM detector, which results in a sawtooth appearance of calibrated spectral profiles. For consistency, the same boxcar filter is also applied to the wavelength set, so as to account for the systematic shift of the I/F profile along the wavelength direction following the odd-even correction.

The first three spectral channels, from 2.00 to 2.02 μm, are never displayed in our plots, since they are affected by large radiometric calibration residuals. The region between 3.76 and 3.85 μm is affected by a permanent instrumental artifact that makes this wavelength range unsuited for data analysis. The increasing I/F value with increasing wavelength beyond 4 μm reveals the thermal contribution provided by hot volcanic spots within the typical size of JIRAM ground footprints.

Figure 1b shows the same spectra as Figure 1a, with the addition of an arbitrary offset on the vertical axis, to facilitate reading. The vertical dashed lines with oblique labels on top mark the position and the confirmed or putative assignment of recurrent spectral features, most of which were already highlighted in the work of Mura et al. (2020) based on Juno/JIRAM data, and which have been discussed in the Introduction. For example, signatures at 2.54 μm, 2.79 μm, 2.92 μm, 3.35 μm, 3.56 μm, 4.07 μm and 4.37 μm are firmly diagnostic of SO_2 frost (another diagnostic signature, located at 3.78 μm, falls in the area affected by the permanent instrumental artifact). The strongest band of SO_2 frost, centered at 4.07 μm, displays an asymmetric shape: not only is it affected by thermal emission on its right shoulder, but it shows inflections at about 4.10 and 4.14 μm, which are consistently observed in different orbits and could be the spectral counterparts of the combination $\nu_1 + \nu_3$ in the isotopic form (isotopologue) $^{34}SO_2$ and of the combination $\nu_1 + \nu_3$ in the isotopic form $^{32}S^{18}O^{16}O$ (Nash and Betts, 1995). From this evidence, we can confirm that on the surface of Io SO_2 frost on the surface of Io likely includes multiple isotopologues, whose fingerprints are revealed in JIRAM data.

The weak signature at 2.10 μm could be ascribed to either SO_2 or CO_2. The signatures at 2.97 and 3.15 μm are very weak and might be suggestive of the potential presence of hydrate compounds trapped within a SO_2 matrix. The signature at 3.92 μm is presumably attributable

to Cl_2SO_2, with a potential contribution of $ClSO_2$ at 4.62 μm. The very weak signature at 4.47 μm could be due to the isotopologue $^{32}S^{16}O^{18}O$, or alternatively to an H_3O^+ overtone/combination in $H_2SO_4 \cdot 4H_2O$. Another very weak signature at 4.55 μm could be the spectral counterpart of the CN bond in nitrile compounds or tholins. Finally, the very weak 2.65-μm band is recurrent in most spectral data sets, even though its source has not yet been positively identified. Similar to Mura et al. (2020), we do not report any absorption feature centered at 3.0 μm, which was pointed out by Douté et al. (2004) and Granahan (2004) on the basis of Galileo/NIMS data. However, it should be noted that some very weak spectral signatures may show up only in higher resolution data and be connected to specific geologic features seen at the local scale. JIRAM data of the Galilean satellites are not outstanding in terms of spatial resolution, and as such they are better suited to perform regional compositional mapping, rather than local compositional investigation.

The signal associated with these average I/F spectra is variable and in first approximation comes from two parameters: the number of spectra acquired in a given sequence and the solar illumination conditions, with more spectra and lower phase angle values favoring a better SNR. On the other hand, the in-flight instrumental noise (NESR) largely comes from two parameters: the dark current (induced by the detector's temperature) and the spectrometer's thermal background signal at long wavelengths (induced by the spectrometer's temperature). In addition to this, Jupiter's radiation environment can generate spurious artifacts in the detector. The in-flight NESR can be effectively calculated from the sky background pixels observed by the spectrometer along with Io observations. These sky background pixels are way more numerous than those covering the target, and, once we exclude those pixels that may be affected by in-field stray-light coming from Io or Jupiter, they are fully representative of the instrumental noise in terms of dark current, spectrometer's temperature, and impinging radiation. Therefore, in each perijove passage, the noise can be derived as the standard deviation of the raw signal (expressed in digital numbers, or DN) measured in all valid sky background pixels, which we convert into a single-spectrum NESR by dividing it by the instrument spectral responsivity. An average NESR spectrum can then be obtained by assuming that, while averaging over a population of N samples (in our case, N independent spectra of Io), the uncertainty decreases with the square root of N. After converting such an average NESR spectrum into I/F units, we find that in most cases the spread in I/F due to the instrumental noise is negligible with respect to systematic errors such as calibration residuals or the odd-even effect. Figure 2 shows the average I/F spectra obtained by JIRAM separately for each orbit, along with the associated variability due to the in-flight noise. In a few specific orbits (17, 18 and 26), this increases longward of 4 μm as a consequence of JIRAM passive radiator's orientation with respect to the direction of Jupiter, inducing a higher thermal background.

For every single I/F profile, in this work we consider the most recurring features located at: 2.10 μm, 2.54 μm, 2.65 μm, 2.79 μm, 2.92 μm, 3.35 μm, 3.55 μm, 3.92 μm, 4.07 μm, 4.37 μm, 4.47 μm, 4.55 μm, and 4.62 μm. The position and shape of these absorption feature can slightly vary from one sequence to another, due to the changing illumination and viewing circumstances. For this reason, for each average I/F spectrum obtained in a given orbit/sequence, we first determine a constant value for the position of the minimum of each absorption band and of its left and right shoulders. We linearly interpolate the spectral continuum between the two wings, we remove it and we finally calculate the band depth (BD) following the formula of Clark and Roush (1984): $D_B = (R_C - R_B)/R_C$, where R_B and R_C are the I/F value at the band minimum and the I/F of the spectral continuum at the same wavelength of the band minimum, respectively. In Table 2, for each absorption feature observed in JIRAM average spectral profiles, we summarize details about the average wavelength values of the

band minimum and of its left and right shoulders, which we use to remove the spectral continuum and compute the band depth.

This way we build a lookup table file, where for each JIRAM pixel that meets our geometric constraints, we keep track of: the filename, the index of the pixel along the slit, the BD values calculated for each spectral signature of interest, and the geometric information related to that specific pixel (latitude and longitude of the pixel center and its four corners, phase angle, solar incidence angle emission angle, and local solar time). In this file, the entire I/F spectrum related to that pixel is also saved. The mapping of the data is therefore done by reading this lookup table, which collects all the valid JIRAM spectroscopic observations of Io. There are 130 spectroscopy files overall, including a total of 1167 useful spectra in the range 2–5 μm (see Table 1).

To map JIRAM data, we considered a grid with fixed angular resolution of 1° both in latitude and in longitude. Since on a great circle of the surface of Io one angular degree corresponds to roughly 32 km, angular bins of 1°×1° are adequate to present JIRAM data, which to date achieved a maximum spatial resolution of ~58 km/px. Starting from the knowledge of the planetocentric coordinates of the four corners for each individual JIRAM pixel, a statistical weight for any ground footprint is defined as the inverse of its projected area, so that data with lower spatial resolution have less weight than data with higher resolution. For each spectral feature of interest, we sum all BD values with related statistical weight falling within a given bin, then we perform a weighted average keeping track of the overall redundancy and statistical weight. This approach ultimately allows us to produce maps that are representative of spectral indices computed for a specific orbit as well as for the entire data set, despite the variable spatial resolution values. We tried the reverse process, i.e. carrying out a weighted average of the spectral profiles in the portion of wavelengths affected by the absorption, and performing the calculation of the BD downstream of this weighted spectral average, obtaining the same results.

For each spectral signature considered here, we evaluate the mean, the standard deviation and the median value of the distribution of the band depth values. For most signatures, the mean and median values are close to each other, testifying a substantially symmetrical distribution. However, for some weak and very weak signatures, e.g. those centered at 3.92, 4.55 and 4.62 μm, the mean and median values are farther apart, and the maximum values are well beyond 3 times the standard deviation, indicating an asymmetrical distribution that is easily the result of low-signal data and/or poor illumination and observation conditions. On the basis of this statistics, we determine an appropriate upper limit for the band depth values to be considered as realistic and retained in our maps, so as to bring the distribution back to a more symmetrical condition. As a result of this filtering, in our maps the spatial coverage of SO_2 frost, which is omnipresent and shows strong absorption bands, may not be matched by the spatial coverage of other chemical species showing much weaker spectral counterparts.

4 Results and Discussion

Figure 3 maps the redundancy of JIRAM data and the statistical weights used to calculate weighted averages for each angular bin. These maps were obtained on the basis of the most prominent SO_2 feature centered at 4.07 μm, which is omnipresent in spectroscopic Io data, so as to ensure that the coverage presented here is the largest achievable with our data set. From the number of filled angular bins, it turns out that the overall coverage obtained by JIRAM on Io under our geometric constraints is 22.4%, of which 14.0% covers the leading hemisphere and 8.4% covers the trailing hemisphere. While this percentage is not outstanding,

particularly with respect to the coverage obtained by Galileo/NIMS, it is meaningful enough to allow us to undertake a preliminary spectroscopic mapping. It should also be noted that latitudes above 75°, both north and south, are not covered, despite JIRAM can always see the polar regions of the satellites. This comes from our choice to discard JIRAM data with solar incidence angle >75°, i.e. the fraction of the dayside close to the terminator. We could easily increase the coverage up to ~90° in latitude, but at the cost of including noisy spectra, in turn inducing worse average spectral profiles and questionable BD mapping results. On the other hand, the coverage in longitude is limited by our choice to discard emission angles greater than 75°, which may suffer from limb proximity (in those sequences/orbits with coarser spatial resolution, this could imply conditions where the JIRAM pixel is not fully illuminated being on the edge of the satellite).

The largest redundancy was achieved in the pro-Jovian, trailing hemisphere, where it was possible to observe some areas on several different orbits, up to a maximum of 8 times, while in most cases the redundancy was much lower, typically between one and two looks of the same area. Similarly, the largest statistical weight (~55%) pertains to the few situations in which JIRAM's ground footprint was comparable with the 1° angular dimension of our bins, whereas in most cases, related to coarser spatial resolution, the weight attributed to ground footprints was typically 5-7%.

Figure 4 shows maps of the weighted average BD values for the most prominent spectral signatures diagnostic of of SO_2 frost in the 2–5 μm range, centered at 4.07, 4.37, 2.79 and 2.54 μm (in decreasing order of strength). The maps are transparently superimposed onto an optical global mosaic of Io, to facilitate association with some of the major geologic features. In general, despite the limited coverage, these maps show that SO_2 frost-related BD values measured in four different diagnostic bands are quite well correlated to each other. The asymmetrical trend already highlighted by Carlson et al. (1997) and Douté et al. (2001) on the basis of Galileo/NIMS data is confirmed: BD values increase in moving away from the equatorial region towards high latitudes, and the leading hemisphere generally shows higher abundance of SO_2 frost compared to the trailing hemisphere, which however has less coverage. JIRAM data highlight a reduction in the abundance of SO_2 frost in the region of Loki patera, the largest Io's volcanic depression, ~200 km-wide, and in the large space between the Ra and Babbar paterae. Conversely, a substantial increase in the strength of SO_2 frost is observed in the southern part of the leading hemisphere, particularly in the large area between Tarsus Regio, which is largely white bright plains material including a couple of paterae (Williams et al., 2011), and Haemus Montes, which is a combination of lineated mountain material and undivided mountain material (Williams et al., 2011). To a lesser extent, SO_2 frost is also enriched also towards Bactria Regio, which is mostly made of layered plains material (Williams et al., 2011). At low latitudes, JIRAM data covering Bosphorous Regio, which surrounds Emakong patera and is classified as bright flow material plus undivided flow material (Williams et al., 2011), display a substantial enrichment in SO_2 frost. In the northern leading hemisphere, an enrichment in SO_2 is observed at latitudes greater than 60° in Chalybes Regio, also classifed as bright flow material and undivided flow material interspersed by red-brown plains material (Williams et al., 2011). Although JIRAM data do not cover Tvashtar patera, a streak of data that reaches towards that geologic feature from southeast, covering a bright flow material unit (Williams et al., 2011), highlights an increasing strength of SO_2 with decreasing distance from Tvashtar, probably due to the presence of a plume ring. In the pro-Jovian trailing hemisphere covered by JIRAM, this latitudinal asymmetry is less prominent; nevertheless an increase in SO_2 frost can be inferred both at southern latitudes in Lerna Regio, which is a mixture of yellow bright plains material and undivided flow material (Williams et

al., 2011), and in a white bright plains material unit north of the Surt volcano (Williams et al., 2011).

One surprising result is the patchy distribution of SO_2 frost in the pro-Jovian hemisphere, both leading and trailing, at northern latitudes. These regions were covered in orbits 17, 18 and 24, which have a relatively good spatial resolution (69-76 km/px) and thus a larger weight in our weighted average, even though orbits 17 and 18 are also noisier longward of ~4 μm. It should be noted that the four SO_2 bands mapped here are the most prominent ones in the 2–5 μm range sampled by JIRAM, and there is a good spatial coherence in BD values computed for different bands, which argues for this mottled distribution to be plausible.

In Figure 5, we map the weighted averaged BD values of the absorption bands centered respectively at 3.92, 4.47, 4.55, and 4.62 μm. The first of these signatures, attributed to sulfuryl chloride (Cl_2SO_2), shows substantial spatial coherence with the SO_2 frost distributions presented in Figure 4. In particular, we note that the depth of this band increases in areas of the leading hemisphere such as Tarsus Regio, Haemus Montes, Bosphorous Regio and southeast of Tvashtar, which also display an enrichment in SO_2. The trailing hemisphere generally shows a weaker BD, particularly in Loki patera, while relatively large abundances are found in Lerna Regio in the southern hemisphere, west of Amaterasu patera and in the white bright plain material unit north of Surt, again consistent with the enhanced SO_2 frost abundance. However, the highest values in the 3.92-μm BD are recorded in the northern, pro-Jovian hemisphere east of Chalybes Regio: here we see no obvious trend on a regional scale due also to sparse coverage; but we report instead a patchy distribution already observed in those same areas for SO_2. It is legitimate to ask whether the maximum values found in the map, corresponding to the yellow and red colors, are the result of particularly noisy data or of a better spatial resolution compared to other sequences, bearing in mind that the presented values have already been filtered by considering the statistics of the entire BD data set and excluding very large deviations from the mean and median values of the distribution.

The 4.47-μm band is very weak and is potentially indicative of a specific isotopologue of the SO_2 molecule, namely $^{32}S^{16}O^{18}O$, or alternatively of the presence of the hydroxonium molecule H_3O^+ in sulfuric acid tetrahydrate, $H_2SO_4 \cdot 4H_2O$. By looking at Figure 1, this feature is not always seen in JIRAM spectra: for example, it is not observed in the average spectral profiles of orbits 18 and 24. Because its spatial distribution is largely coherent with the distribution of SO_2 frost in most JIRAM data, and since the 4.07-μm band displays inflections that could be diagnostic of multiple isotopic forms of SO_2, our maps favor a connection of this spectral feature with the isotopologue $^{32}S^{16}O^{18}O$.

The 4.55-μm band might be the spectral counterpart of the CN bond in nitrile compounds or tholins. In this case, and although the band is quite persistent in the I/F spectral profiles measured by JIRAM, according to our map it is hard to highlight any obvious trend on most of the covered surface, even after filtering plausible BD values. Most of these BD values are definitely less than 0.1 because this is a very weak band, and the largest values are achieved only in very specific places, mainly located in the northern hemisphere but sometimes also in the southern hemisphere, such as southeast of Ra patera and in other localized patches, not related to particularly noisy data.

Finally, the band centered at 4.62 μm is attributable to $ClSO_2$ as a potential additional contributor to the Cl_2SO_2, although in principle it could also be due to the presence of a carbon-nitrogen carrier. Again, this is a very weak band, and the spatial distribution highlights that spatial coherence with the distribution of the 3.92-μm band is achieved only in specific regions: particularly in Tarsus Regio, Media Regio, Bosphorous Regio, southeast of Tvashtar, and to a lesser extent in Lerna Regio. However, the 4.62-μm BD is also enhanced in the large region

between Loki patera and Ra patera, unlike the 3.92-μm band. So, if the interpretation of $ClSO_2$ were correct, this compound would not be associated with Cl_2SO_2 everywhere. It is interesting to note that also in this case, extreme values in terms of BD show up particularly in the pro-Jovian hemisphere, close to the prime meridian.

Figure 6 shows maps of weighted averaged, BD values computed for the 2.1-μm band, attributable to SO_2 or alternatively to CO_2, and the 2.65-μm band, compared with the 4.07-μm SO_2 frost band and 3.92-μm Cl_2SO_2 band bands, discussed before.

The 2.1-μm band is weak but recurrent, although it does not clearly show up in all orbits (looking at Figure 1b, it is just barely seen in orbits 5, 20 and 26). In most cases, BD values are less than 0.1, but there is no clear spatial coherence with respect to the prominent SO_2-frost bands detected longward of 2.5 μm. If this band is more easily explained by the $3\nu_1 + \nu_3$ combination of SO_2 frost compared to the $2\nu_3$ overtone of CO_2, as suggested by Schmitt et al. (1994), there should be a general spatial coherence with the distribution obtained for other stronger SO_2 signatures, most notably those displayed in Figure 4. Instead this does not appear to be the case in JIRAM-derived maps, since even in areas that show a clear enhancement in SO_2 frost, such as Tarsus Regio, Haemus Montes and Bosphorous Regio, there is no evidence for a corresponding increase in the depth of the 2.1-μm band. On the contrary, in the pro-Jovian hemisphere (both leading and trailing), and mainly in the northern hemisphere, we report an increase of this BD value over specific areas, which does not follow any regional trend but at the same time does not appear to be the result of a random ("salt and pepper") distribution as could result from particularly noisy or problematic data. Enhancements in the 2.1-μm band depth are local rather than regional. A north-south asymmetry emerges from our map, with the northern hemisphere displaying higher BD values compared to the southern hemisphere. One question that arises is therefore whether an alternative explanation for this band can come back into favor, e.g. CO_2 as first proposed by Sandford et al. (1991, 1993), which may be easily outgassed during volcanic activity. Another question is: why do we observe latitudinal rather than longitudinal asymmetries in the abundance of this compound? Is this similar to the latitudinal asymmetry in SO_2 frost first identified by Douté et al. (2001) and attributed to transport of volatiles from plumes? Is the observed abundance permanent or transient?

In the 2–5 μm range, pure CO_2 ice would display stronger signatures at 4.26, 2.70 and 2.78 μm, where the JIRAM average spectral profiles show only inflections or extremely weak bands (the 2.79-μm band of SO_2 frost completely masks a potential CO_2 signature at 2.78 μm). Furthermore, the sublimation temperature of CO_2 is well below the average daytime surface temperature of Io (~110 K). For these reasons, it is hard to support the detection of CO_2 in JIRAM data; although it should be noted that the daytime temperatures decrease in moving away from the equator to the poles, emphasizing the possibility that high-latitude regions, which are colder, may act as cold traps for those volatile compounds that would have a short lifetime at low latitudes.

Figure 6c maps the depth of the spectral signature at 2.65 μm, which was first reported by Mura et al. (2020) on the basis of JIRAM spectroscopic data obtained in the early Juno orbits. From Figure 1b it emerges how this band is weaker than the 2.1-μm band, and extremely weak in particular in the average I/F profiles of the orbits 20 and 26, which, however, also show a lower average signal level. The 2.65-μm map shows regions where the BD values increase in a spatially coherent way rather than randomly, which is one evidence in support of the fact that this feature is real and not due to an instrumental artifact. The distribution is comparable to that of the 2.1-μm band in that there seems to be no substantial spatial coherence with the distribution of SO_2 frost, especially where the latter is most abundant. One exception to this rule is Bosphorous Regio, which is SO_2-rich and where the 2.65-μm BD values rise up

to ~6%. Values up to ~4% are found in a relatively broad region around Loki patera, which is classified as yellow bright plains material (Williams et al., 2011), east of Media Regio, which is a combination of yellow bright plains material and undivided flow material (Williams et al., 2011), and in part of Chalybes Regio. A latitudinal trend shows up, with low-to-intermediate latitudes displaying higher BD values compared to high latitudes. Extreme BD values are patchy and unrelated with large geologic features, but perhaps correlated with specific local-scale features in the pro-Jovian hemisphere. Several questions arise: what is the absorber responsible for the 2.65-µm band? Are the two bands at 2.1 µm and 2.65 µm connected to each other? Why are they both very weak or absent in the southern hemisphere? Since the southern hemisphere of Io has more Prometheus-type plumes, which are SO_2-rich and longer lasting than Pele-type plumes, could it be that SO_2 deposition from plumes would cover or mask other deposits?

Indeed, laboratory spectra acquired by Salama et al. (1990) demonstrated that a thin film of H_2S displays a very weak signature at 2.69 µm, interpreted as the $\nu_1 + \nu_2$ combination of this molecule, which moves to shorter wavelengths (2.67 µm) when H_2S is mixed with SO_2. Pure H_2S ice, as well as a thin layer of pure H_2S superimposed on an SO_2 substrate, is extremely unstable at the typical daytime surface temperatures of Io (Schmitt & Rodriguez, 2003). Furthermore, H_2S diluted in SO_2 would give rise to a stronger band at 3.85 µm, which does not fit with NIMS data and unfortunately falls within JIRAM's permanent artifact region. Because H_2S gas is an expected product of volcanism, its detection on the surface of Io is important, especially if it had a transient character. In this regard, it cannot be excluded that H_2S can condense and survive at low concentrations for a time sufficient for JIRAM to reveal it in some of the close passages of Juno.

To quantify the correlation existing between different spectral indices, most notably those diagnostic of SO_2 frost and those assigned to other putative compounds, we have produced scatterplots that relate pairs of BD values. Figure 7 shows a first series of these scatterplots, displaying the depth of the 2.65-µm band versus the depth of other spectral signatures, tentatively fitted by a linear model. First of all, we observe that in some scatterplots the points concentrate in relatively compact clusters, while in other scatterplots the spread is larger. These plots can safely exclude that the absorber responsible for the 2.65-µm spectral feature is related to the abundance of SO_2 frost as revealed by its strongest signature centered at 4.07 µm. The 2.65-µm vs. 4.07-µm scatterplot even points to a potential anti-correlation between these two compounds, meaning that the 2.65-µm absorber is mostly not trapped within an SO_2-frost matrix. Similarly, no substantial correlation arises between the BD values measured for the 2.1-µm and 2.65 µm bands, and little correlation exists between the BD values measured for the 2.65-µm and 3.92-µm bands, which suggests that the compounds responsible for the absorptions at 2.10, 2.65 and 3.92 µm should be different. Indeed, a larger degree of correlation is found between the 2.65-µm spectral signature and the very weak 4.62-µm absorption band, which may be due to $ClSO_2$. BD maps displayed in Figures 5 and 6 actually point out that there is spatial coherence for different spectral signatures in some specific regions, but this is not the common rule.

Figure 8 shows a second series of scatterplots, which are meant to verify whether the 2.1-µm band is actually correlated with other spectral features diagnostic of SO_2 frost in the 2–5 µm range. In doing so, we not only check the correlation between the two band depths at 2.1 and 4.07 µm, the latter being the strongest SO_2-frost signature. In fact, grain size plays an important role in the depth of an absorption band, and previous work demonstrated how the granularity of SO_2 frost actually changes across the surface of Io (Douté et al., 2001). For this reason, we also evaluate the correlation existing between the depth of the 2.1-µm band and the weak SO_2-frost band centered at 2.54 µm, as well as the very weak bands centered at 3.35 µm

and 3.55 μm. In all of these cases, and regardless of the relative strength of the spectral signatures being considered, no significant correlation emerges, which would suggest that another compound is responsible for the 2.1-μm absorption. One might speculate that the left shoulder of the 2.1-μm band, which we estimate at 2.06 μm (see Table 2), could be affected by significant calibration residuals, although previous works based on JIRAM spectroscopic observations of the Galilean satellites used the spectral range down to 2.02 μm with no particular issues (Filacchione et al., 2019; Mura et al., 2020). However, it should also be noted that the coverage so far obtained from JIRAM spectroscopic data is still relatively small, although it is sufficient to derive trends on a regional scale for about one fifth of the satellite surface. It is therefore fair enough to state that the correlations shown here are indicative of a large portion of the Io's pro-Jovian hemisphere.

Figure 9 shows a third and last series of scatterplots. Two of those scatterplots relate BD values measured for the 3.92-μm band to those of the 4.07-μm and 4.62-μm bands. In the 3.92 vs. 4.07-μm scatterplot, the determination coefficient (i.e., the squared correlation coefficient R^2) has a value of ~0.16, which is reasonable since a higher abundance of SO_2 may favor the formation of Cl_2SO_2. The correlation between the 3.92-μm band and the 4.62-μm band is much weaker, which confirms what previously found in Figure 5, i.e. if the 4.62-μm band is diagnostic of $ClSO_2$, then it is associated with the more abundant Cl_2SO_2 not everywhere, but only in specific areas. One interesting result comes from the scatterplot of the BD at 4.47 μm vs. 4.07 μm, which also shows a determination coefficient value of ~0.10. This is indicative of a non-negligible degree of correlation between the intensity of the band at 4.47 μm and the abundance of SO_2 frost on the surface, in support of the evidence that sulfur dioxide actually exists in several isotopic forms on the surface of Io, including $^{32}S^{16}O^{18}O$. Finally, we have related the BD values measured for the 4.62-μm and 4.55-μm bands, following the hypothesis that both these signatures might be due to a carbon-nitrogen carrier. Although the determination coefficient is less than 0.1, it is nevertheless greater than others found for the linear fit models of scatterplots shown in Figure 7, Figure 8 and Figure 9. This result is interesting, because it indicates that in addition to $ClSO_2$, the 4.62-μm band might also be linked to the presence of nitrile compounds or tholins on the surface, which had been previously proposed to exist on Callisto and Ganymede.

5 Concluding remarks

In the three-year period between March 2017 and April 2020, the JIRAM spectro-imager onboard the Juno spacecraft was able to obtain useful spectroscopic data of Io on nine out of twenty-six orbits, at pixel resolutions ranging between 58 and 162 km and at latitudes up to 75° both north and south, having ruled out data with very large solar incidence angles. These data, covering the spectral range 2–5 μm, show different diagnostic spectral signatures of SO_2 frost and other compounds identified or proposed on the basis of over forty years of previous observations and laboratory experiments (Figure 1). In this paper, we used the JIRAM spectroscopic data set so far available to attempt a mapping of the depth values for a number of absorption features, including some very weak bands that had not previously been detected by the NIMS imaging spectrometer onboard the Galileo mission. While the overall JIRAM spectroscopic data set of Io does not have a spatial resolution adequate enough to reveal any connection between very weak spectral signatures and specific local-scale geologic features, it can highlight regional trends, characterize the surface composition of large geologic features, and reveal compositional details of regions of interest whose size is comparable with the typical JIRAM pixel resolution.

The mapping obtained for SO_2 frost, which is omnipresent at the spatial scales investigated by JIRAM, achieves ~22% coverage of the surface, with a clear prevalence of the

pro-Jovian hemisphere compared to the anti-Jovian hemisphere (Figure 3). Consistent with previous NIMS findings, JIRAM data confirms broadly regional trends related to SO_2 frost, which is increasingly abundant in moving away from the equator to intermediate and high latitudes, and is enhanced in the leading hemisphere compared to the trailing hemisphere, which, however, is less covered by JIRAM (Figure 4). In the leading hemisphere, the geologic regions showing the largest abundance of SO_2 frost are: Haemus Montes, Tarsus Regio, Bactria Regio, Bosphorous Regio, one region southeast of Tvashtar patera, and part of Chalybes Regio. In the trailing hemisphere, the region of Loki patera and Ra patera, as well as the large space between Ra patera and Babbar patera, are depleted in SO_2, whereas Lerna Regio and a white bright plain material unit north of Surt are SO_2-rich. In the pro-Jovian hemisphere, at northern latitudes, JIRAM shows an enhancement of SO_2 in restricted areas, on the basis of spectroscopic data that were acquired in three orbits, with spatial resolution in the range 69-76 km/px. Spatial coherence is observed in this mottled distribution between different signatures diagnostic of SO_2 frost, and a similar, but not equal, mottled distribution is detected for other weaker absorption bands, which argues for this distribution to be real rather than the result of a much larger instrumental noise.

The coverage obtained by JIRAM, although limited, is meaningful enough to undertake a preliminary mapping for weak or very weak spectral features. Our results show that in the areas covered by JIRAM, i.e. mostly the pro-Jovian hemisphere, the 2.1-μm band is unrelated with other spectral features located at longer wavelengths and firmly diagnostic of SO_2 frost, regardless of their relative strength (see Figures 6a, 6b and Figure 8), but at the same time cannot support the possibility that this may be a CO_2 signature, due to the substantial lack of other stronger features diagnostic of CO_2 in the 2–5 μm range. The 2.65-μm band, reported by Mura et al. (2020) on the basis of JIRAM data, is also unrelated or even anti-correlated with SO_2 frost (Figures 6 and 7), which points to some absorber not intimately mixed within an SO_2 frost matrix. One possibility would be H_2S, which is unstable at the typical daytime surface temperatures of Io but may survive long enough to be detected by JIRAM during Juno's close passages to Jupiter, e.g. in the large, yellow bright plains material surrounding Loki and in Bosphorous Regio. Also, the two bands at 2.1 μm and 2.65 μm are not correlated with each other, indicating that they are not due to the same compound.

The distribution of the two bands at 2.1 μm and 2.65 μm, although different, suggests the existence of a latitudinal trend, in which extreme band depth values are mostly recorded in the northern hemisphere compared to the southern hemisphere, especially at intermediate to high latitudes, but with a patchy rather than uniform pattern. If volatile compounds are responsible for these two absorptions, it is plausible that, similar to SO_2, a condensation and remobilization cycle favors a net transport of volatiles towards high latitudes, where surface temperatures are colder. However, a different type of volcanic activity, with Prometheus-type plumes erupting for several years, compared to Pele-type plumes that are usually short-lived, could also erase the signatures of these compounds in specific regions, explaining an uneven distribution in a broad range of spatial scales.

JIRAM results confirm the association of sulfuryl chloride Cl_2SO_2, suggested to be the best candidate for the 3.92-μm absorption, with SO_2 frost; but at the same time they indicate that the contribution of $ClSO_2$, possibly responsible for the 4.62 μm absorption, may be relevant only in specific regions, rather than everywhere (Figures 5 and 9). Both the spectral profiles measured by JIRAM and the maps related to the distribution of the 4.47-μm band show that this is very likely the spectral fingerprint of a specific isotopologue of SO_2 ($^{32}S^{16}O^{18}O$), therefore confirming that on the surface of Io sulfur dioxide actually exists in several isotopic forms (Figures 5b and 9c). Finally, it is worth noting that the very weak spectral signatures at 4.55 and 4.62 μm, which are recurrently observed in the JIRAM spectra, could indicate the

presence, even at very low concentrations, of nitrile compounds or tholins, already reported on the surfaces other Galilean satellites (Figures 5c, 5d and 9d).

While this preliminary work does not claim to answer many of the open questions about Io's surface composition, it demonstrates JIRAM's ability to investigate the Galilean satellite showing the largest wealth of spectral information. Compared to Earth-based telescopic observations, JIRAM's observations of Io occur with a relatively high frequency and, pending the approval of an extended Juno mission, the coverage of Io by JIRAM will supposedly increase in the future, possibly at spatial resolutions better than those obtained in the prime mission.

Acknowledgments and Data availability

JIRAM is funded by the Italian Space Agency (ASI), ASI-INAF contract 2016-23-H.0. The JIRAM instrument was built by Selex ES, under the leadership of the Italian National Institute for Astrophysics, Institute for Space Astrophysics and Planetology (INAF-IAPS), Rome, Italy. JIRAM is operated by INAF-IAPS, Rome, Italy. Support of the Juno Science and Operations Teams is gratefully acknowledged. Part of this work was supported by the Mainstream INAF project: "*Caratterizzazione delle superfici dei satelliti di Giove mediante osservazioni di Juno-JIRAM e misure di laboratorio nell'infrarosso*" (INAF grant 1.05.01.86.11). Part of this work was carried out at the Jet Propulsion Laboratory, California Institute of Technology, under contract with NASA.

JIRAM data are archived in NASA's Planetary Data System (PDS) and may be found at: https://pds-atmospheres.nmsu.edu/data_and_services/atmospheres_data/JUNO/jiram.html. Spectral calibration parameters of JIRAM-SPE measured during the on-ground calibration campaign are partly reported in Section 4.2 of Adriani et al. (2017). The instrumental responsivity coming from the radiometric calibration is discussed in Sections 4.4 and 4.5 of Adriani et al. (2017), where spectral responsivity profiles measured during the on-ground calibration campaign are also shown. The entire analysis presented in this work was performed using homemade software developed in the commercial IDL language (https://www.harrisgeospatial.com/Software-Technology/IDL). Datasets for this research are available in this in-text data citation reference: Tosi et al. (2020), DOI: https://doi.org/10.5281/zenodo.3923699.

References

Acton, C. H. (1996). *Ancillary data services of NASA's navigation and ancillary information facility. Planet. Space Sci. 44*(1), 65–70. doi: 10.1016/0032-0633(95)00107-7.

Adriani, A., Moriconi, M. L., Mura, A., Tosi, F., Sindoni, G., Noschese, et al. (2016). *Juno's Earth flyby: the Jovian InfraRed Auroral Mapper preliminary results. Astrophys. Space Sci. 361*(8), id.272. doi: 10.1007/s10509-016-2842-9.

Adriani, A., Filacchione, G., Di Iorio, T., Turrini, D., Noschese, R., Cicchetti, A., et al. (2017). *JIRAM, the Jovian InfraRed Auroral Mapper. Space Sci. Rev. 213*(1–4), 393–446. doi: 10.1007/s11214-014-0094-y.

Baklouti, D., Schmitt, B., & Brissaud, O. (2008). *S_2O, polysulfuroxide and sulfur polymer on Io's surface? Icarus 194*(2), 647–659. doi: 10.1016/j.icarus.2007.11.016.

Bolton, S. J., Lunine, J., Stevenson, D., Connerney, J. E. P., Levin, S., Owen, T. C., et al. (2017). *The Juno Mission. Space Sci. Rev. 213*(1–4), 5-37. doi: 10.1007/s11214-017-0429-6.

Brown, R. H (1974). *Io – Jupiter's surprising satellite. New Scientist 64*, 484–487.

Carlson, R. W., Weissman, P. R., Smythe, W. D., & Mahoney, J. C. (1992). *Near-Infrared Mapping Spectrometer experiment on Galileo. Space Sci. Rev. 60*(1–4), 457–502. doi: 10.1007/BF00216865. 457–502.

Carlson, R. W., Smythe, W. D., Lopes-Gautier, R. M. C., Davies, A. G., Kamp, L. W., Mosher, J. A., et al. (1997). *Distribution of sulfur dioxide and other infrared absorbers on the surface of Io. Geophys. Res. Lett. 24*(20), 2479–2490. doi: 10.1029/97GL02609.

Carlson, R. W., Kargel, J. S., Douté, S., Soderblom, L. A., & Dalton, J. B. (2007). *Io's surface composition*. From: Io After Galileo: A New View of Jupiter's Volcanic Moon (R. M. C. Lopes and J. R. Spencer, Eds.), Springer Praxis Books. Springer, Berlin, Heidelberg, pp. 193–229. doi: 10.1007/978-3-540-48841-5_9.

Clark, R. N., & Roush, T. L. (1984). *Reflectance spectroscopy: quantitative analysis techniques for remote sensing applications. J. Geophys. Res. 89*(B7), 6329–6340. doi: 10.1029/JB089iB07p06329.

Cruikshank, D. P. (1980). *Infrared spectrum of Io, 2.8-5.2 μm. Icarus 41*, 240–245. doi: 10.1016/0019-1035(80)90007-X.

Cruikshank, D. P., Howell, R. R., Fanale, F. P., & Geballe, T. R., 1985. *Sulfur dioxide ice on Io*. In: "Ices in the Solar System"; Proceedings of the Advanced Research Workshop, Nice, France, January 16-19, 1984 (A86-23051 09-91). D. Reidel Publishing Co, Dordrecht, pp. 805–815.

de Kleer, K., McEwen, A. S., Park, R., et al. (2019). *Tidal Heating: Lessons from Io and the Jovian System, Final Report for the Keck Institute for Space Studies*. https://www.kiss.caltech.edu/final_reports/Tidal_Heating_final_report.pdf

Douté, S., Schmitt, B., Lopes, R., Carlson, R., Soderblom, L., Shirley, J., & the Galileo NIMS Team (2001). *Mapping SO_2 frost on Io by the modeling of NIMS hyperspectral images. Icarus 149*(1), 107–132. doi: 10.1006/icar.2000.6513.

Douté, S., Lopes, R., Kamp, L. W., Carlson, R., Schmitt, B., & the Galileo NIMS Team (2002). *Dynamics and evolution of SO_2 gas condensation around Prometheus-like volcanic plumes on Io as seen by the Near Infrared Mapping Spectrometer. Icarus 158*(2), 460–482. doi: 10.1006/icar.2002.6889.

Douté, S., Lopes, R., Kamp, L. W., Carlson, R., & Schmitt, B. (2004). *Geology and activity around volcanoes on Io from the analysis of NIMS spectral images. Icarus 169*(1), 175–196. doi: doi: 10.1016/j.icarus.2004.02.001.

Fanale, F. P., Brown, R. H., Cruikshank, D. P., & Clark, R. N. (1979). *Significance of absorption features in Io's IR reflectance spectrum. Nature 280*(5725), 761–763. doi: 10.1038/280761a0.

Feaga, L. M., McGrath, M., & Feldman, P. D. (2009). *Io's dayside SO_2 atmosphere. Icarus 201*(2), 570–584. doi: 10.1016/j.icarus.2009.01.029.

Filacchione, G., Adriani, A., Mura, A., Tosi, F., Lunine, J. I., Raponi, A., et al. (2019). *Serendipitous infrared observations of Europa by Juno/JIRAM. Icarus 328*, 1–13. doi: 10.1016/j.icarus.2019.03.022.

Granahan, J. C., 2004. *The detection of iron sulfide on Io. 35th Lunar and Planetary Science Conference*, March 15-19, 2004, League City, Texas, abstract no.1872.

Howell, R. R., Cruikshank, D. P., & Fanale, F. P. (1984). *Sulfur dioxide on Io: Spatial distribution and physical state. Icarus 57*(1) 83–92. doi: 10.1016/0019-1035(84)90010-1.

Howell, R. R., Nash, D. B., Geballe, T. R., & Cruikshank, D. P. (1989). *High-resolution infrared spectroscopy of Io and possible surface materials. Icarus 78*(1), 27–37. doi: 10.1016/0019-1035(89)90067-5.

Lellouch, E., Paubert, G., Moses, J. I., Schneider, N. M., & Strobel, D. F. (2003). *Volcanically emitted sodium chloride as a source for Io's neutral clouds and plasma torus. Nature 421*(6918), 45–47. doi: 10.1038/nature01292.

McCord, T. B., Carlson, R. W., Smythe, W. D., Hansen, G. B., Clark, R. N., Hibbitts, C. A., et al. (1997). *Organics and other molecules in the surfaces of Callisto and Ganymede. Science 278*(5336), 271–275. doi: 10.1126/science.278.5336.271.

McCord, T. B., Hansen, G. B., Clark, R. N., Martin, P. D., Hibbitts, C. A., Fanale, F. P., et al. (1998). *Non-water ice constituents in the surface material of the icy Galilean satellites from the Galileo Near-Infrared Mapping Spectrometer investigation. J. Geophys. Res. 103*(E4), 8603-8626. doi: 10.1029/98JE00788.

McGrath, M. A., Belton, M. J. S., Spencer, J. R., & Sartoretti, P. (2000). *Spatially resolved spectroscopy of Io's Pele plume and SO_2 atmosphere. Icarus 146*(2), 476–493. doi: 10.1006/icar.1999.6412.

Moore, M. H., Hudson, R. L., & Carlson, R. W. (2007). *The radiolysis of SO_2 and H_2S in wate ice: implications for the icy Jovian satellites. Icarus 189*(2), 409–423. doi: 10.1016/j.icarus.2007.01.018.

Moullet, A., Lellouch, E., Moreno, R., Gurwell, M., Black, J. H., & Butler, B. (2013). *Exploring Io's atmospheric composition with APEX: First measurement of $^{34}SO_2$ and tentative detection of KCl. Astrophys. J. 776*(1), article id. 32. doi: 10.1088/0004-637X/776/1/32.

Mura, A., Adriani, A., Tosi, F., Lopes, R. M. C., Sindoni, G., Filacchione, et al. (2020). *Infrared observations of Io from Juno. Icarus 341*, id. 113607. doi: 10.1016/j.icarus.2019.113607.

Nash, D. B., & Betts, B. H. (1995). *Laboratory infrared spectra (2.3–23 μm) of SO_2 phases: applications to Io surface analysis. Icarus 117*(2), 402–419. doi: 10.1006/icar.1995.1165.

Nash, D. B., & Betts, B. H. (1998). *Ices on Io – composition and texture*. In: Schmitt, B., De Bergh, C., Festou, M. (Eds.), Solar System Ices. Kluwer, Dordrecht, pp. 607–638. doi:10.1007/978-94-011-5252-5_25.

Noschese, R., Cicchetti, A., Sordini, R., Cartacci, M., Mura, A., Brooks, S. M., et al. (2020). *Juno/JIRAM: Planning and commanding activities. Adv. Space Res. 65*(1), 598–615. doi: 10.1016/j.asr.2019.09.052.

Postberg, F., Kempf, S., Srama, R., Green, S. F., Hillier, J. K., McBride, N., & Grün, E. (2006). *Composition of Jovian dust stream particles. Icarus 183*(1), 122–134. doi: 10.1016/j.icarus.2006.02.001.

Salama, F., Allamandola, L. J., Witteborn, F. C., Cruikshank, D. P., Sandford, S. A., & Bregman, J. D. (1990). *The 2.5-5.0 micron spectra of Io – evidence for H_2S and H_2O frozen in SO_2. Icarus 83*(1), 66–82. doi: 10.1016/0019-1035(90)90006-U.

Sandford, S. A., Salama, F., Allamandola, L. J., Trafton, L. M., Lester, D. F., & Ramseyer, T. F. (1991). *Laboratory studies of the newly discovered infrared band at 4705.2 cm^{-1} (2.1253 μm) in the spectrum of Io: The tentative identification of CO_2. Icarus 91*(1), 125–144. doi: 10.1016/0019-1035(91)90132-D.

Sandford, S. A., & Allamandola, L. J. (1993). *Ices Containing SO_2, H_2S, and CO_2: Implications for Io. Icarus 106*(2) 478–488. doi: 10.1006/icar.1993.1186.

Schmitt, B., de Bergh, C., Lellouch, E., Maillard, J., Barbe, A., & Douté, S. (1994). *Identification of three absorption bands in the 2-μm spectrum of Io. Icarus 111*(1), 79–105. doi: 10.1006/icar.1994.1135.

Schmitt, B., & Rodriguez, S. (2003). *Possible identification of local deposits of Cl_2SO_2 on Io from NIMS/Galileo spectra. J. Geophys. Res. 108*(E9), CiteID 5104. doi: 10.1029/2002JE001988.

Smythe, W. D., Nelson, R. M., & Nash, D. B. (1979). *Spectral evidence for SO_2 frost or adsorbate on Io's surface. Nature 280*(5725), 766–767. doi: 10.1038/280766a0.

Soderblom, L. A., Becker, K. J., Becker, T. L., Carlson, R. W., Davies, A. G., Kargel, J. S., et al. (1999). *Deconvolution of Galileo NIMS day-side spectra of Io into thermal, SO_2, and non-SO_2 components*. 30th Annual Lunar and Planetary Science Conference, March 15-29, 1999, Houston, TX, abstract no. 1901.

Spencer, J. R., Jessup, K. L., McGrath, M. A., Ballester, G. E., & Yelle, R. (2000). *Discovery of gaseous S_2 in Io's Pele plume. Science 288*(5469), 1208–1210. doi: 10.1126/science.288.5469.1208.

Srama, R., Ahrens, T. J., Altobelli, N., Auer, S., Bradley, J. G., Burton, M., et al. (2004). *The Cassini Cosmic Dust Analyzer. Space Sci. Rev. 114*(1–4), 465–518. doi: 10.1007/s11214-004-1435-z.

Tosi, F., Mura, A., Lopes, R. M. C., Filacchione, G., Ciarniello, M., Zambon, F., et al. (2020). Data for the research article: "Mapping Io's Surface Composition with Juno/JIRAM". Zenodo. doi: https://doi.org/10.5281/zenodo.3923699.

Trafton, L. M., Lester, D. F., Ramseyer, T. F., Salama, F., Sandford, S. A., & Allamandola, L. J. (1991). *A new class of absorption feature in Io's near-infrared spectrum. Icarus 89*(2), 264–276. doi. 10.1016/0019-1035(91)90178-V.

Williams, D. A., Keszthelyi, L. P., Crown, D. A., Yff, J. A., Jaeger, W. L., Schenk, P. M., et al. (2011). *Geologic map of Io: U.S. Geological Survey Scientific Investigations Map 3168, scale 1:15,000,000*, 25 p., available at https://pubs.usgs.gov/sim/3168/.

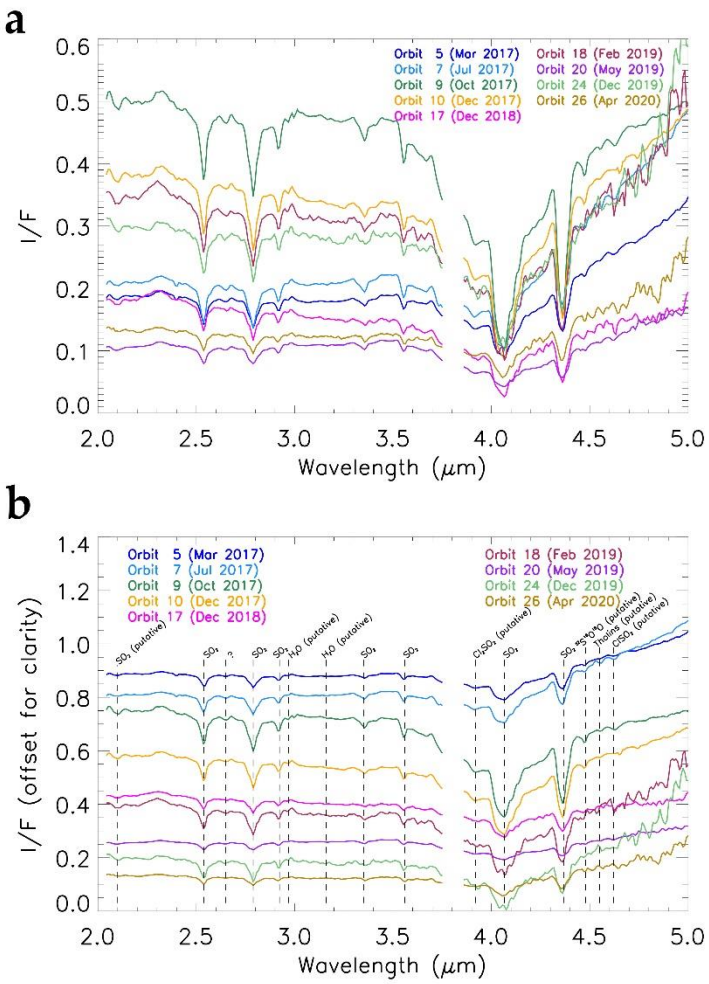

Figure 1. a. Average spectral profiles of Io as observed by JIRAM during nine different orbits around Jupiter, from March 2017 (orbit 5) to April 2020 (orbit 26). The profiles are expressed in units of calibrated radiance factor (I/F) in the 2–5 μm spectral range, without any photometric correction. The first three spectral channels, from 2.00 to 2.02 μm, are not shown due to large calibration residuals. A gap between 3.76 and 3.85 highlights the spectral counterpart of a junction connecting two order sorting filters placed above the detector, resulting in a permanent instrumental artifact. **b.** Same profiles as panel **a**, with the addition of an arbitrary offset in the Y axis to facilitate reading. The dashed vertical lines highlight the wavelengths corresponding to the center of the most recurrent spectral signatures observed in the JIRAM spectra, located at: 2.10 μm, 2.54 μm, 2.65 μm, 2.79 μm, 2.92 μm, 2.97 μm, 3.16 μm, 3.35 μm, 3.55 μm, 3.92 μm, 4.07 μm, 4.37 μm, 4.47 μm, 4.55 μm, and 4.62 μm.

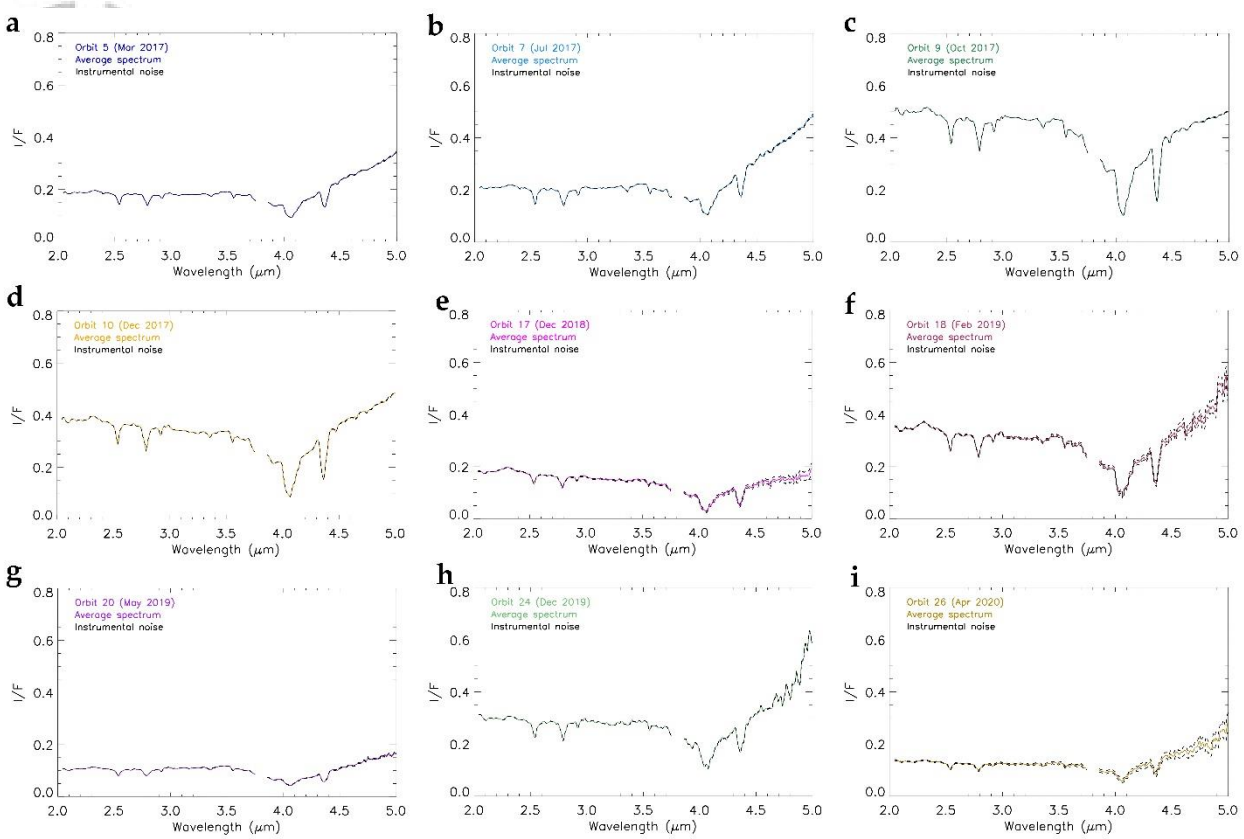

Figure 2. Average spectral profiles of Io obtained by JIRAM in the nine different orbits considered in this work, shown together with their associated 1-sigma NESR variability (black dashed line) (panels **a-i**). For each average spectrum (orbit), colors are consistent with Figure 1. In-flight instrumental noise is usually negligible compared to the target's signal, but may increase longward of 4 μm in specific orbits as a consequence of a higher spectrometer's thermal background signal.

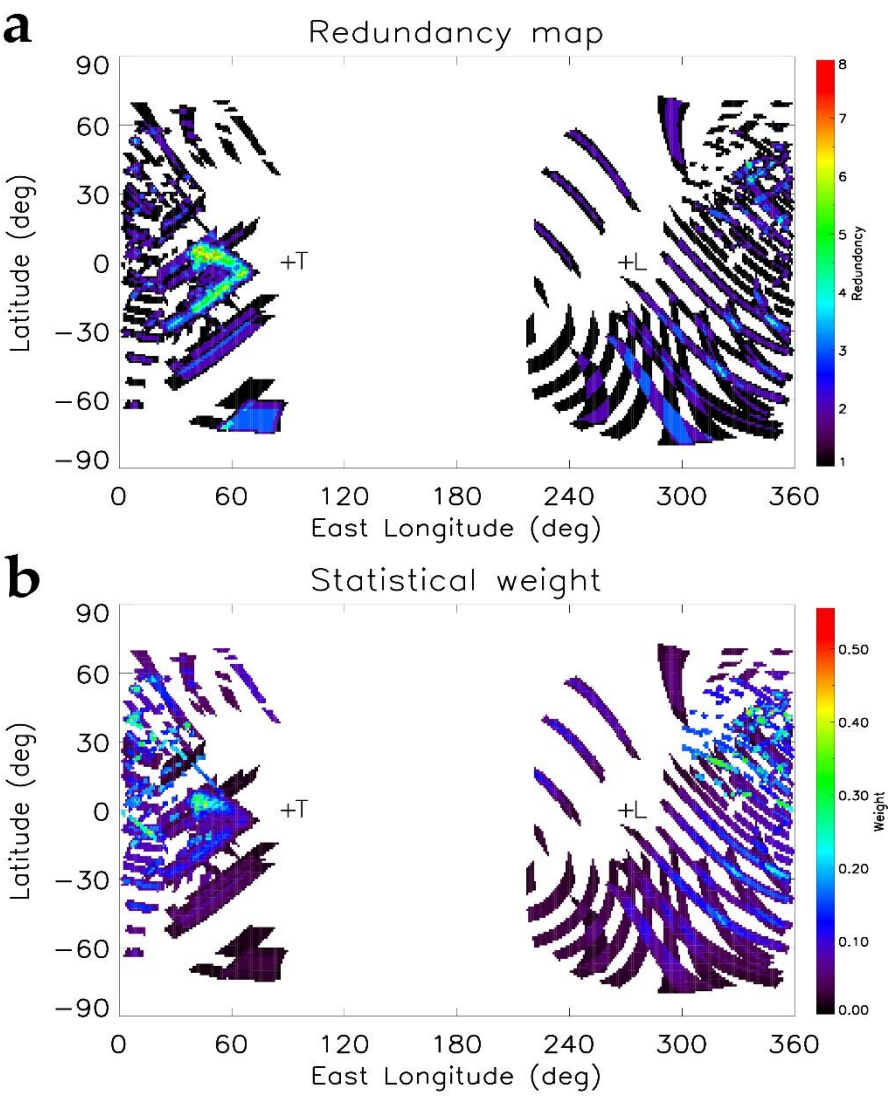

Figure 3. a. Map of redundancy in the JIRAM coverage of the Io surface, having considered 1°×1° angular bins. The symbols "+*T*" and "+*L*" mark the apex of the trailing and leading hemispheres, respectively. By including data from all of the nine Juno orbits considered here, the overall coverage is ~22%. Latitudes above 75° both north and south are not covered due to our conservative choice to discard all JIRAM data acquired with solar incidence angle values >75°. In most cases, a given region is observed from 1 to 2 times, while redundancy is pushed to higher values (revealed by the green to red colors) in a much smaller number of cases, which are found in the trailing hemisphere at low latitudes, due to recurrent conditions met during flybys. **b.** Map of statistical weights used to perform a weighted average of JIRAM-derived spectral indices. For each angular bin including JIRAM data, the weight of those data is defined as the inverse of the projected area of the ground footprint. This way, observations with high spatial resolution, comparable with that of the angular bins, have a greater weight than observations at low resolution where a single ground footprint covers several angular bins.

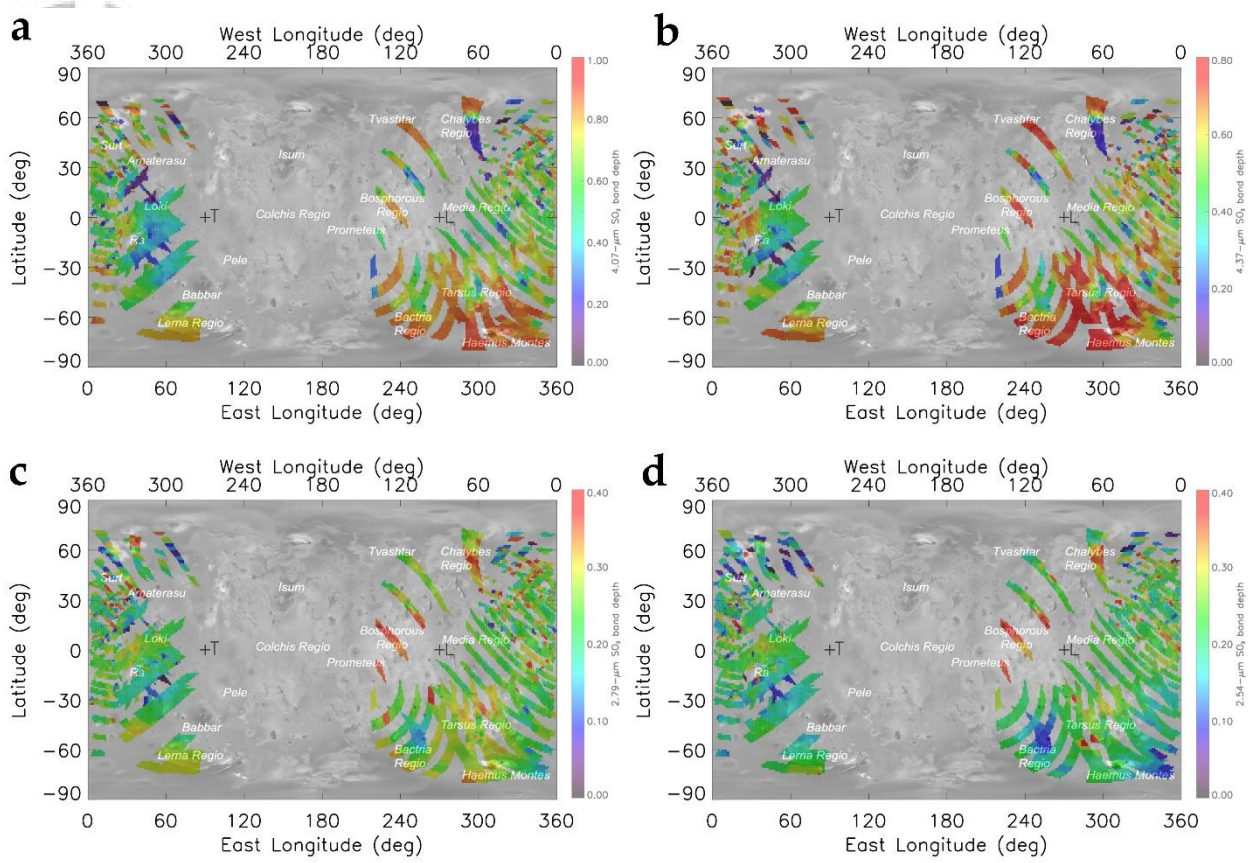

Figure 4. Spatial distribution of the depth of the strongest absorption bands diagnostic of SO_2 frost, revealed between 2.5 and 4.5 μm. **a.** Map of band depth for the main SO_2 band, centered at 4.07 μm. **b.** Map of band depth for the 4.37-μm signature. **c.** Map of band depth for the 2.79-μm absorption. **d.** Map of band depth for the 2.54-μm feature. The maps derived from the weighted averages of JIRAM-derived band depths are transparently superimposed on an optical mosaic of the Io surface, to facilitate association with some of the major geologic formations. Color bars have different ranges in different panels, because the absorption bands at 4.07 μm and 4.37 are much stronger than the bands at 2.79 and 2.54 μm. In all maps presented in this figure and in the following ones, the horizontal axes express both east and west longitudes, so as to enable a quick comparison with past results, which used west longitudes, but also facilitate a comparison with the data that will be acquired by future space missions such as JUICE and Europa Clipper, which may favor eastward longitudes. The "+*T*" and "+*L*" symbols mark the apex of the trailing and leading hemispheres, respectively.

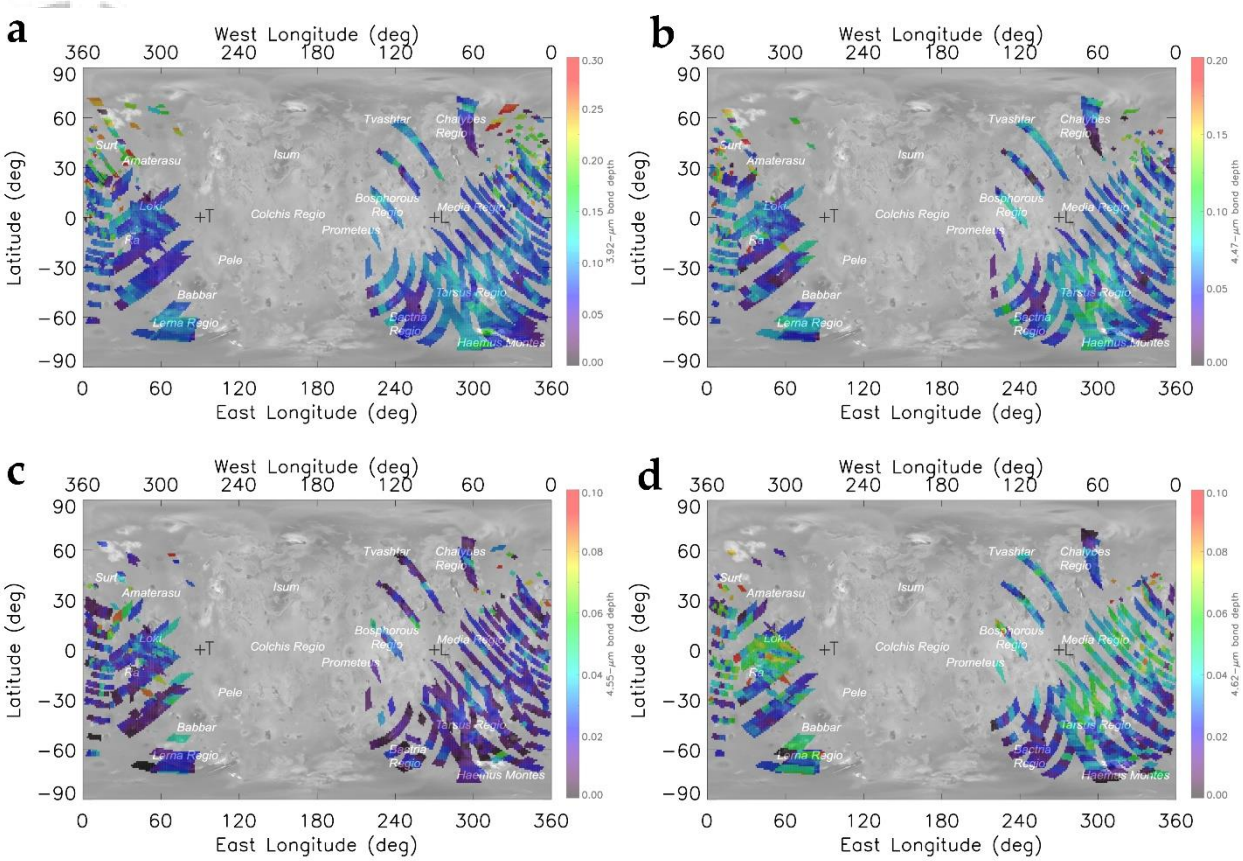

Figure 5. Spatial distribution of JIRAM-derived band depth values for the spectral signatures centered respectively at 3.92 μm (panel **a**), 4.47 μm (panel **b**), 4.55 μm (panel **c**), and 4.62 (panel **d**). These absorption bands are frequently observed in JIRAM spectra, but are much weaker than the bands diagnostic of SO_2 frost. For this reason, the BD values are generally lower, with most values below 0.1. The mismatches that are observed in the coverage between different maps are due to the filtering performed on the BD values (revealed by the range of the color bar), with the purpose of excluding outlier values that are too far from the mean and median values of the overall distribution.

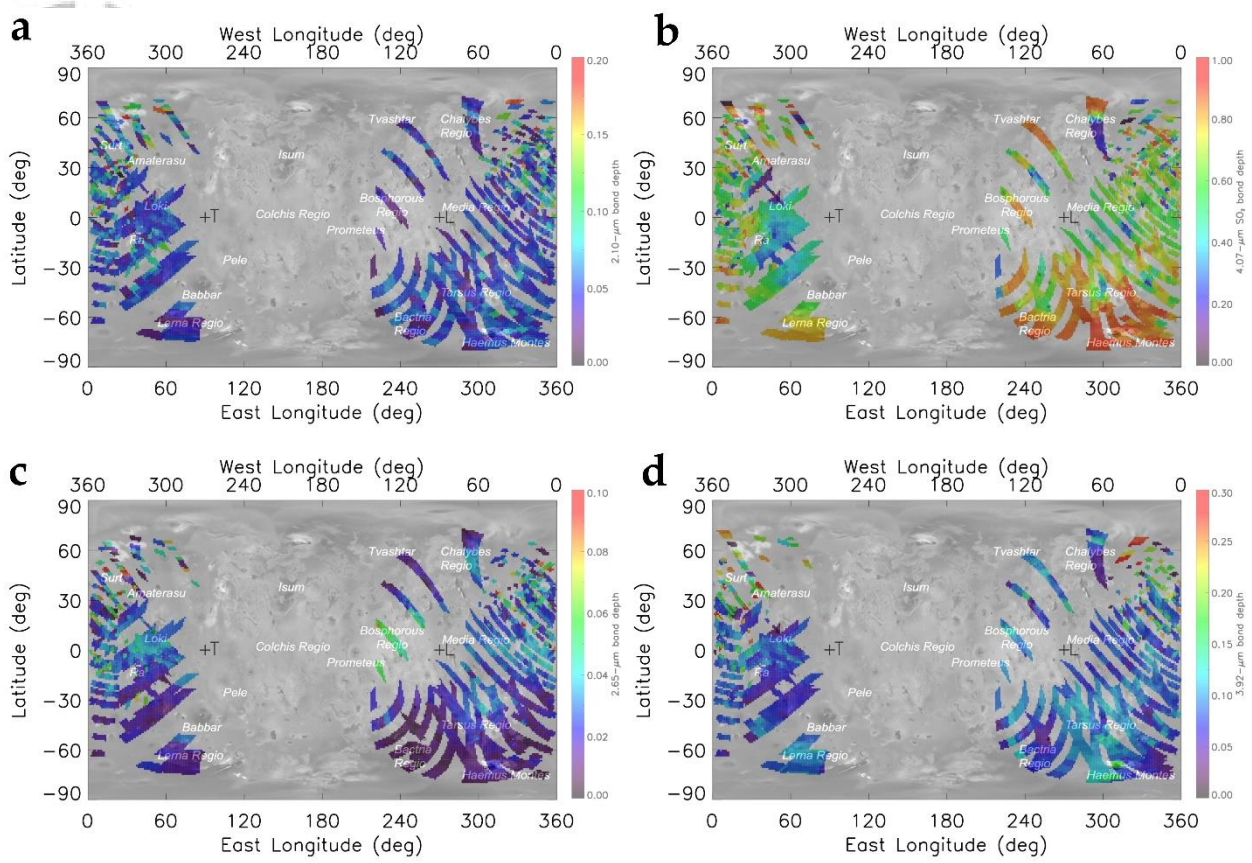

Figure 6. Spatial distribution of the band depth values calculated for the absorption bands centered at 2.1 μm (panel **a**), 4.07 μm (panel **b**), 2.65 μm (panel **c**), and 3.92 μm (panel **d**). While the 2.1-μm band has been observed since 1991, the 2.65-μm band is weaker, has been observed only recently on the basis of Juno/JIRAM data, and do not correspond to wavelengths affected by known instrumental artifacts. A direct comparison between panels **a**, **c** and panels **b**, **d** can help in qualitatively establish any coherence between the 2.1-μm and 2.65-μm BD maps and those derived for SO_2 frost and Cl_2SO_2, respectively.

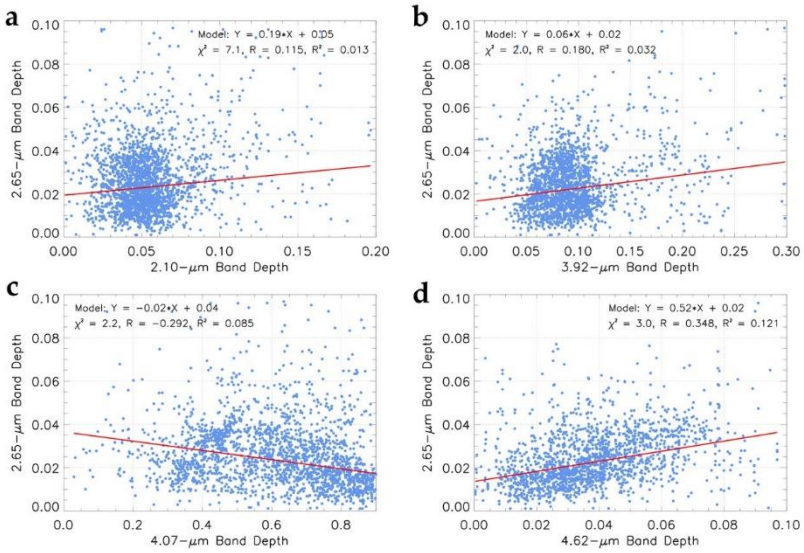

Figure 7. Scatterplots related to the BD values measured for: 2.65 μm band vs. 2.10 μm band (panel **a**), 2.65 μm band vs. 3.92 μm band (panel **b**), 2.65 μm band vs. 4.07 μm band (panel **c**), and 2.65 μm band vs. 4.62 μm band (panel **d**). In each scatterplot, a linear fit model (red line) is superimposed on the distribution. The values of the chi-square (χ^2), the Pearson correlation coefficient (R), and the coefficient of determination (i.e., the squared correlation coefficient R^2) coming from the linear fit are also reported. These scatterplots are meant to evaluate if and how much the 2.65-μm band, first reported by Mura et al. (2020) on the basis of JIRAM data, is correlated with other chemical species whose existence is ascertained or suggested on the surface of Io.

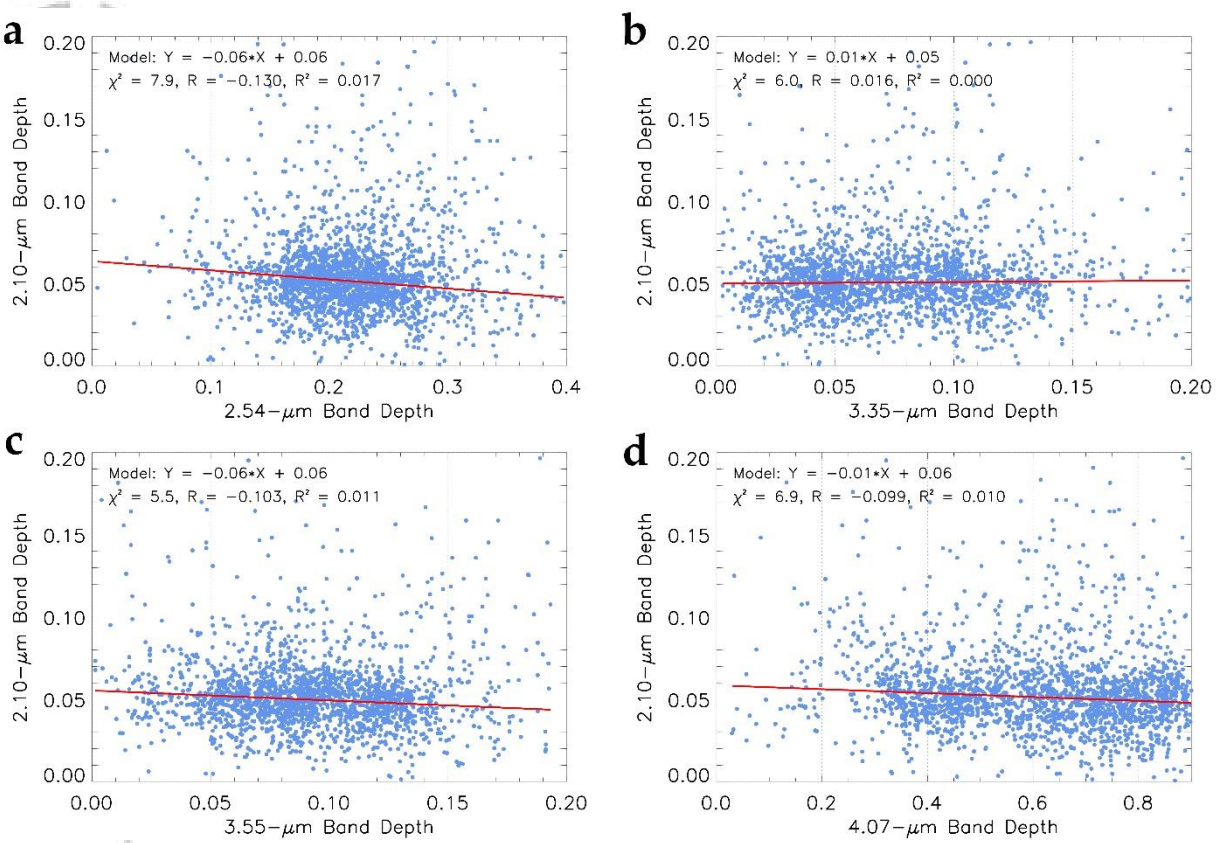

Figure 8. Scatterplots related to the BD values measured for: 2.10 μm band vs. 2.54 μm band (panel **a**), 2.10 μm band vs. 3.35 μm band (panel **b**), 2.10 μm band vs. 3.55 μm band (panel **c**), and 2.10 μm band vs. 4.07 μm band (panel **d**). In each scatterplot, a linear fit model (red line) is superimposed on the distribution. The values of the chi-square (χ^2), the Pearson correlation coefficient (R), and the coefficient of determination (i.e., the squared correlation coefficient R^2) coming from the linear fit are also reported. These scatterplots are meant to evaluate whether and how much the very weak band centered at 2.1 μm, usually attributed to sulfur dioxide, is related to other bands of the same compound located at longer wavelengths. In doing so, and to avoid that our results be substantially affected by grain size effects, we consider not only the strongest band centered at 4.07 μm, but also the weak band at 2.54 μm and those, even weaker, centered at 3.35 and 3.55 μm, whose relative strength is comparable to that of the 2.1-μm band.

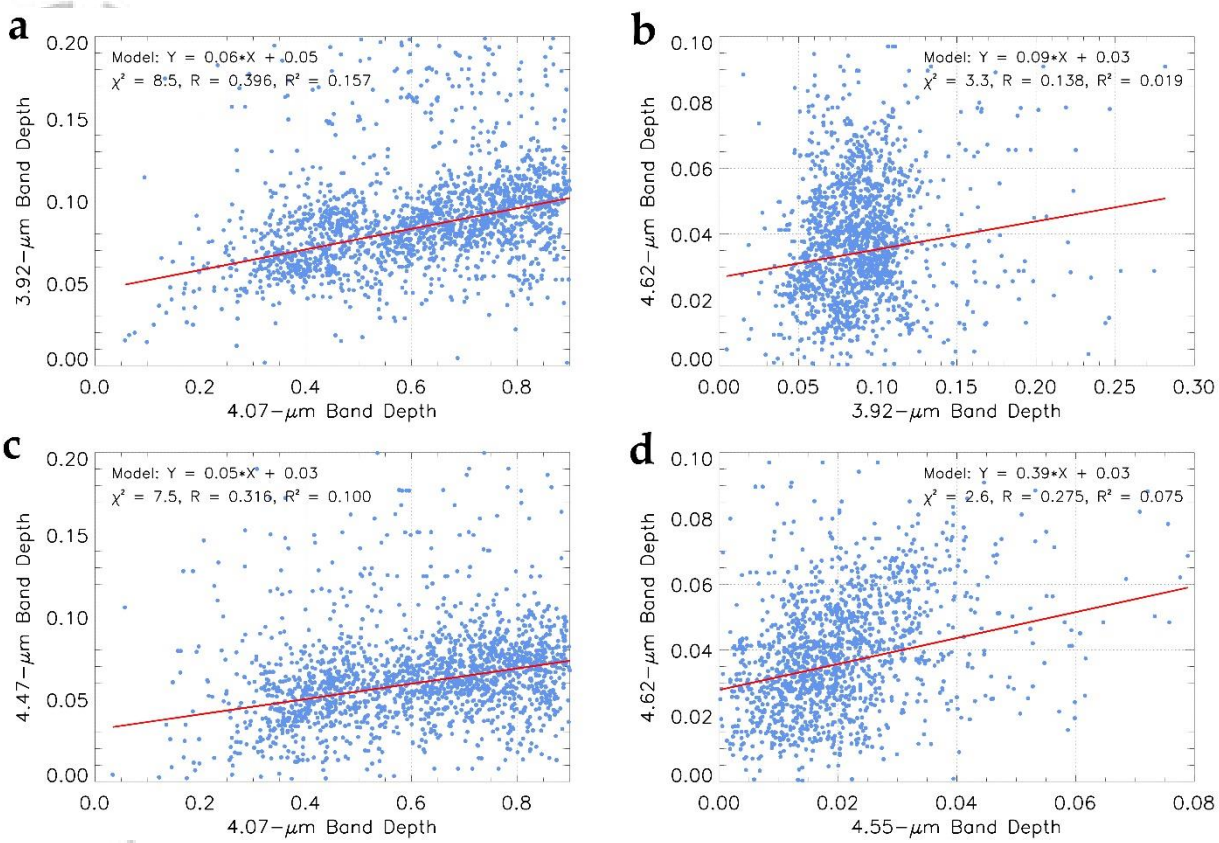

Figure 9. Scatterplots related to the BD values measured for: 3.92 μm band vs. 4.07 μm band (panel **a**), 4.62 μm band vs. 3.92 μm band (panel **b**), 4.47 μm band vs. 4.07 μm band (panel **c**), and 4.62 μm band vs. 4.55 μm band (panel **d**). In each scatterplot, a linear fit model (red line) is superimposed on the distribution. The values of the chi-square (χ^2), the Pearson correlation coefficient (R), and the coefficient of determination (i.e., the squared correlation coefficient R^2) coming from the linear fit are also reported. These scatterplots are meant to evaluate the correlations existing between the absorption band at 3.92 μm, presumably due to sulfuryl chloride Cl_2SO_2, and the absorption band at 4.47 μm, with respect to sulfur dioxide SO_2. In addition to this, we also evaluate the correlation existing between the absorber at 4.62 μm, possibly $ClSO_2$ or alternatively sulfates or cyanides, and the absorber at 4.55 μm, potentially due to the CN bond in nitrile compounds or tholins.

Table 1. Summary of JIRAM spectroscopic data of Io used in this work. Each row reports the characteristics of the data sequence acquired close to an orbit's perijove in terms of: duration of the spectroscopic observations, number of files, number of spectra, JIRAM pixel resolution in the sub-spacecraft point, planetocentric coordinates of the sub-spacecraft point (minimum, maximum and mean values of latitude and longitude), and solar illumination and observation conditions (minimum, maximum and mean values for: solar phase angle, solar incidence angle, and emission angle), as well as the range of local solar times.

Sequence	Start time [UTC]	Stop time [UTC]	N. of files	N. of spectra	JIRAM pixel resolution in the sub-spacecraft point (min, max, mean) [km/px]	Sub-spacecraft latitude (min, max, mean) [deg]	Sub-spacecraft longitude (min, max, mean) [deg]	Solar phase angle (min, max, mean) [deg]	Solar incidence angle (min, max, mean) [deg]	Emission angle (min, max, mean) [deg]	Local solar time (min, max, mean) [h]
JM0051	2017-03-27T11:20:31	2017-03-27T12:12:11	18	108	142.5, 161.7, 153.2	28.0°S, 27.0°S, 27.6°S	356.1°E, 358.9°E, 357.4°E	96.2°, 98.7°, 97.4°	27.3°, 74.7°, 56.7°	24.1°, 73.9°, 50.9°	7.0, 11.7, 8.9
JM0071	2017-07-10T16:41:37	2017-07-10T17:09:15	10	52	97.4, 102.1, 99.7	50.8°N, 53.4°N, 52.1°N	171.1°E, 181.7°E, 176.6°E	109.1°, 110.4°, 109.8°	38.5°, 75.0°, 61.8°	36.2°, 74.4°, 55.8°	7.1, 12.2, 9.4
JM0091	2017-10-24T19:47:30	2017-10-24T20:02:10	21	365	102.2, 103.5, 102.9	38.5°S, 35.1°S, 36.8°S	355.7°, 355.9°E, 355.8°E	54.0°, 56.8°, 55.4°	2.7°, 74.9°, 45.9°	2.0°, 75.0°, 38.9°	8.2, 16.9, 13.6
JM0101	2017-12-17T00:03:31	2017-12-17T00:17:20	14	118	111.5, 113.5, 112.5	77.7°S, 77.6°S, 77.6°S	35.8°E, 46.6°E, 41.2°E	90.1°, 92.6°, 91.3°	17.9°, 75.0°, 55.3°	17.1°, 75.0°, 47.4°	7.2, 16.7, 12.5
JM0171	2018-12-21T12:16:35	2018-12-21T12:30:15	8	103	68.7, 72.0, 70.5	46.4°N, 48.9°N, 47.6°N	283.5°E, 287.8°E, 285.3°E	88.2°, 89.3°, 88.8°	21.0°, 74.8°, 54.5°	15.1°, 72.7°, 44.5°	7.4, 14.1, 10.5
JM0181	2019-02-12T13:33:02	2019-02-12T13:40:05	12	137	71.1, 72.6, 71.8	42.4°N, 43.3°N, 42.9°N	297.7°E, 300.2°E, 298.9°E	82.7°, 84.7°, 83.9°	14.4°, 74.9°, 50.7°	11.9°, 73.9°, 43.5°	7.2, 14.8, 10.4
JM0201	2019-05-29T06:59:34	2019-05-29T07:10:15.48	19	60	106.6, 110.9, 108.7	18.1°N, 18.7°N, 18.4°N	349.5°E, 351.8°E, 350.6°E	118.6°, 121.6°, 120.2°	48.2°, 74.3°, 63.4°	47.5°, 73.5°, 60.7°	7.0, 8.8, 7.8
JM0241	2019-12-26T13:36:39	2019-12-26T13:55:24	25	156	72.7, 76.0, 74.4	33.2°N, 35.0°N, 34.1°N	56.0°E, 62.5°E, 59.1°E	84.8°, 87.8°, 86.3°	17.3°, 74.8°, 49.6°	17.8°, 74.7°, 50.0°	10.6, 16.7, 14.1

JM0261	2020-04-10T11:19:54	2020-04-10T11:25:57	3	68	58.4, 59.6, 59.0	39.9°N, 41.1°N, 40.5°N	343.7°E, 346.4°E, 345.0°E	60.6°, 61.5°, 61.1°	17.8°, 73.8°, 47.5°	4.2°, 73.4°, 39.5°	7.2, 15.4, 10.9

Table 2. Summary of spectral features observed in JIRAM average I/F spectral profiles of Io. For each absorption feature, we report the wavelength position of the band minimum and of its left and right shoulders, which we used to compute the band depth after continuum removal. We also specify the assignment (be it firm or suggested/presumed) and the strength relative to the spectral continuum. The spatial distribution of the two very weak absorption features centered at 2.97 and 3.15, marked by an asterisk, is not discussed in this work. Conversely, we discuss the behavior and potential assignment of the very weak band centered at 2.65 μm, first reported by Mura et al. (2020).

Band minimum (μm)	**Left shoulder (μm)**	**Right shoulder (μm)**	**Assignment**	**Relative strength**
2.10	2.06	2.14	SO_2 $3\nu_1+\nu_3$ combination (preferred to CO_2 $2\nu_3$ overtone)	Very weak
2.54	2.49	2.59	SO_2 overtone $3\nu_3$	Weak
2.65	2.62	2.67	Unknown (discussed in this work)	Very weak
2.79	2.73	2.84	SO_2 combination $2\nu_1+\nu_3$	Medium
2.92	2.89	2.95	SO_2 overtone $3\nu_1$	Very weak
2.97*	2.95	2.98	H_2O stretch ν_3 (suggested)	Very weak
3.15*	3.14	3.18	H_2O stretch ν_1 (suggested)	Very weak
3.35	3.30	3.40	SO_2 combination $\nu_1+\nu_2+\nu_3$	Very weak
3.56	3.52	3.58	SO_2 combination $2\nu_1+\nu_2$	Very weak
3.92	3.88	3.97	Cl_2SO_2 combination $\nu_1+\nu_6$ (best candidate)	Weak
4.07	3.98	4.16	SO_2 combination $\nu_1+\nu_3$	Very strong
4.36	4.31	4.42	SO_2 overtone $2\nu_1$	Strong
4.47	4.45	4.50	$^{32}S^{16}O^{18}O$ isotopologue (suggested), or H_3O^+ overtone/ combination in $H_2SO_4 \cdot 4H_2O$ (suggested)	Very weak
4.55	4.54	4.58	C≡N functional group in tholins and/or nitriles (suggested)	Very weak
4.62	4.60	4.67	$ClSO_2$ overtone $2\nu_2$ (suggested), or some form	Very weak

			of sulfate or cyanides (suggested)	